nature immunology

Drugs and drug-like molecules can modulate the function of mucosal-associated invariant T cells

Andrew N Keller[1,2,8], Sidonia B G Eckle[3,8], Weijun Xu[4,5,8], Ligong Liu[4,5], Victoria A Hughes[1,2], Jeffrey Y W Mak[4,5], Bronwyn S Meehan[3], Troi Pediongco[3], Richard W Birkinshaw[1], Zhenjun Chen[3], Huimeng Wang[3], Criselle D'Souza[3], Lars Kjer-Nielsen[3], Nicholas A Gherardin[3,6], Dale I Godfrey[3,6], Lyudmila Kostenko[3], Alexandra J Corbett[3], Anthony W Purcell[1], David P Fairlie[4,5,9], James McCluskey[3,9] & Jamie Rossjohn[1,2,7,9]

The major-histocompatibility-complex-(MHC)-class-I-related molecule MR1 can present activating and non-activating vitamin-B-based ligands to mucosal-associated invariant T cells (MAIT cells). Whether MR1 binds other ligands is unknown. Here we identified a range of small organic molecules, drugs, drug metabolites and drug-like molecules, including salicylates and diclofenac, as MR1-binding ligands. Some of these ligands inhibited MAIT cells *ex vivo* and *in vivo*, while others, including diclofenac metabolites, were agonists. Crystal structures of a T cell antigen receptor (TCR) from a MAIT cell in complex with MR1 bound to the non-stimulatory and stimulatory compounds showed distinct ligand orientations and contacts within MR1, which highlighted the versatility of the MR1 binding pocket. The findings demonstrated that MR1 was able to capture chemically diverse structures, spanning mono- and bicyclic compounds, that either inhibited or activated MAIT cells. This indicated that drugs and drug-like molecules can modulate MAIT cell function in mammals.

The locus encoding human leukocyte antigen (HLA) molecules is highly polymorphic, which enables HLA molecules to present a broad array of peptide antigens, an essential requirement for protective immunity. Conversely, certain HLA allotypes are often associated with aberrant T cell reactivity, including autoimmunity and food- and drug-linked hypersensitivity[1–3]. Humans also have an array of monomorphic antigen-presenting molecules that have distinct and specialized roles in immunity[4]: the CD1 family is well suited to bind lipid-based antigens[5], while the MHC-class-I-related molecule MR1 presents microbial products associated with vitamin-B2 synthesis for recognition by MAIT cells[6]. Whether MR1 or CD1 can present small-molecule drugs or drug-like molecules to induce an immune response remains unclear.

MAIT cells are an evolutionary conserved subset of innate-like T cells found in many mammals[7,8]. Although the function of MAIT cells is emerging, they are considered to have key roles in immunity[9–11]. MAIT cells are abundant in humans, representing up to 10% of the total T cell population in the blood[12]. MAIT cells mostly express a TCR with an 'invariant' TCR α-chain (TRAV1-2 recombined with TRAJ33, TRAJ20 or TRAJ12) paired with a limited array of TCR β-chains[8,13,14]. MR1 molecules can present stimulatory pyrimidines and non-stimulatory pyrimidine analogs associated with vitamin B2 and vitamin B9, respectively, for surveillance by MAIT cells. For example, some uracils and lumazines derived from riboflavin biosynthesis activate MAIT cells, whereas derivatives of folic acid, including 6-formylpterin (6-FP), are non-stimulatory ligands[15,16]. A key difference between those stimulatory antigens and non-stimulatory antigens is that the former have a ribityl chain that mediates contacts with the TCR on the MAIT cell (the 'MAIT TCR')[17]. After being activated via their TCRs, MAIT cells rapidly secrete an array of pro-inflammatory cytokines, proliferate and have the ability to kill bacterially infected cells[18,19]. It is therefore important to understand the range of ligands that can modulate MAIT cell function.

Through the use of *in silico* discovery approaches, we have identified potential MR1-binding ligands, including some commonly prescribed drugs and drug-like molecules. Furthermore, we evaluated these ligands for their ability to modulate MAIT cell function through their interaction with MR1. We found that some ligands caused upregulation of MR1 expression on the cell surface and inhibited the activation of MAIT cells, while others activated MAIT cells. Consequently, we demonstrate that MR1 can capture chemically diverse scaffolds. These observations indicate that some drugs and drug-like molecules affect MAIT cell function.

[1]Infection and Immunity Program and Department of Biochemistry and Molecular Biology, Biomedicine Discovery Institute, Monash University, Clayton, Australia. [2]ARC Centre of Excellence in Advanced Molecular Imaging, Monash University, Clayton, Australia. [3]Department of Microbiology and Immunology, Peter Doherty Institute for Infection and Immunity, University of Melbourne, Parkville, Australia. [4]Institute for Molecular Bioscience, The University of Queensland, Brisbane, Australia. [5]ARC Centre of Excellence in Advanced Molecular Imaging, University of Queensland, Brisbane, Australia. [6]Australian Research Council Centre of Excellence in Advanced Molecular Imaging, University of Melbourne, Melbourne, Australia. [7]Institute of Infection and Immunity, Cardiff University School of Medicine, Cardiff, UK. [8]These authors contributed equally to this work. [9]These authors jointly directed this work. Correspondence should be addressed to D.P.F. (d.fairlie@imb.uq.edu.au), J.M. (jamesm1@unimelb.edu.au) or J.R. (jamie.rossjohn@monash.edu).

Received 26 February 2016; accepted 3 January 2017; published online 6 February 2017; doi:10.1038/ni.3679

RESULTS

In silico prospecting for MR1 ligands

Published studies have identified uracil analogs, including 5-(2-oxopropylideneamino)-6-D-ribitylaminouracil (5-OP-RU), and pterin or pteridine analogs (such as 6-FP) as agonists and inhibitors, respectively, of the activation of MAIT cells[15]. These compounds contain simple pyrimidine heterocycles as scaffolds, which suggests that the ligand-binding site of MR1 (the A′-pocket) has a propensity to bind small molecules, possibly including drugs, drug-like molecules or fragments[16].

To identify other chemical scaffolds able to bind to MR1, we conducted multiple *in silico* screens in parallel using various chemical libraries, including 6,000 in-house organic compounds and 1,216 drugs (approved by the US Food and Drug Administration (FDA)) from the Distributed Structure–Searchable Toxicity database to target the A′-pocket (**Fig. 1**). On the basis of binding to MR1 by the most active known MAIT cell antigen (5-OP-RU), we performed fragment-based virtual screening of the 6,000-compound library to identify small aromatic aldehydes or carboxylates that might neutralize the charge of the important Schiff-base-forming Lys43 residue of MR1, as well as to identify simple pyrimidines, quinones and enones (**Fig. 1a**), to occupy the same site of MR1 to which 5-OP-RU binds (**Fig. 1b**). This led to 147 hits, including those presented here (**Fig. 1c**). Additionally, a database of 1,216 FDA-approved drugs was screened *in silico* (**Fig. 1d**) for

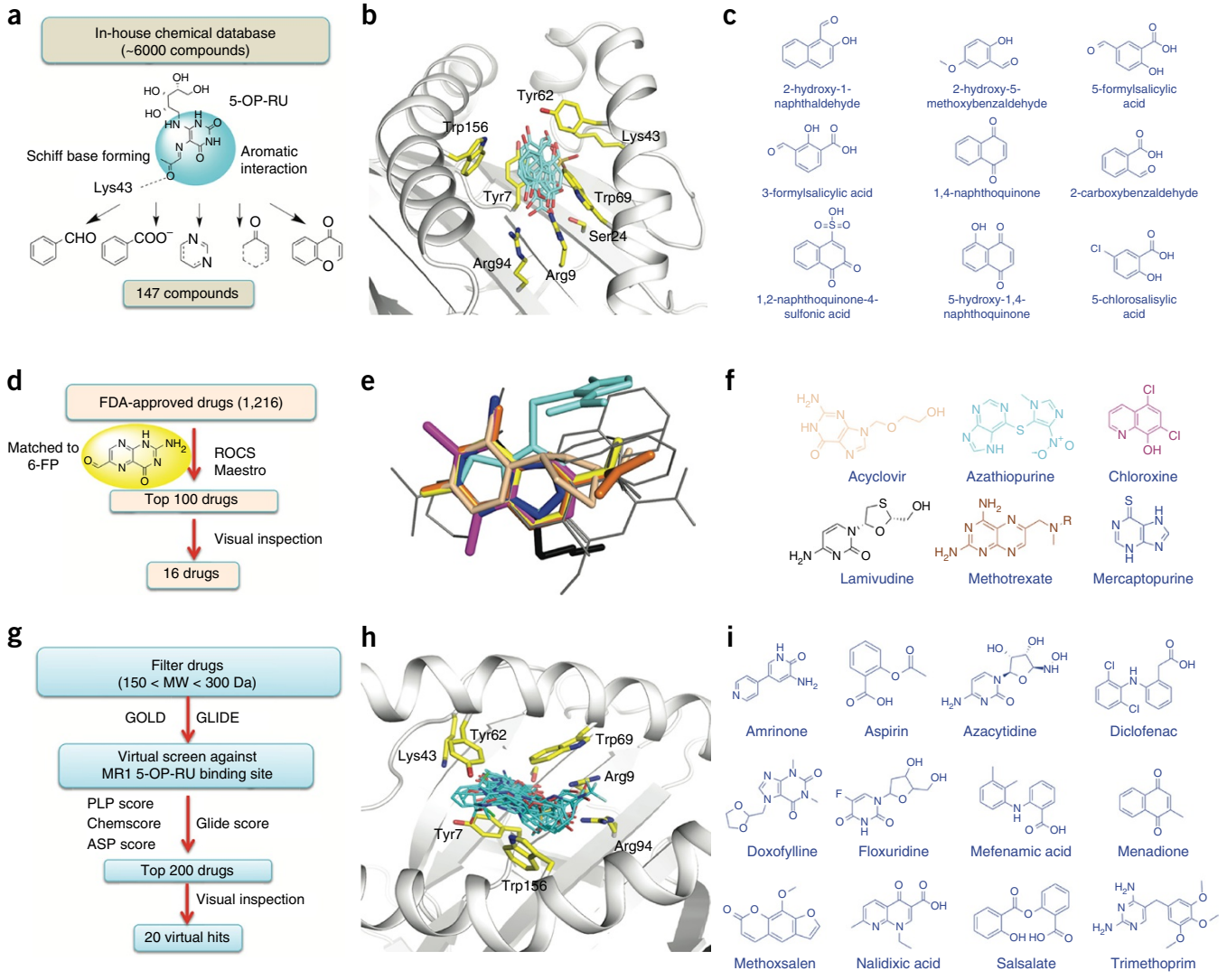

Figure 1 *In silico* virtual screening for putative MR1 ligands. (**a**) Fragment-based *in silico* virtual screen of an in-house chemical database (top) for the selection of compounds relating to fragments of 5-OP-RU. (**b**) Docking-simulated binding 'poses' (cyan) of selected fragments identified as in **a** into MR1 at the binding site of 5-OP-RU; amino acids and positions noted (yellow sticks) are in the MR1 binding site. (**c**) Examples of virtual hits in **b** from the fragment-based screen in **a**. (**d**) Shape-based *in silico* virtual matching (with ROCS and Maestro software) of a pool of drugs (top) to 6-FP as a structural template, followed by visual examination of the 100 top-ranked drugs (ranked on the basis of shape similarity) to determine the extent to which they matched the shape of 6-FP. (**e**) Superimposition of the drugs identified in **d** onto the shape of 6-FP. (**f**) Examples of drugs identified as virtual hits from the shape-based screen in **d**; colors correspond to those of the superimposed structures in **e**. (**g**) Receptor-based virtual screen for the identification of drug hits as putative MR1-binding ligands, beginning with pre-filtering of drugs on the basis of molecular weight (MW) (top), followed by screening *in silico* for predicted binding with the GOLD and GLIDE programs, then ranking with the ChemPLP, Chemscore and ASPscore scoring functions of GOLD, as well as assignment of scores by GLIDE Score, followed by visual examination of the 200 top-scoring drugs for their docked poses within the MR1 binding site. (**h**) Docked poses of 20 virtual hits (cyan) from a subset of the pre-filtered drug database in **g** in the putative ligand-binding site in MR1 defined by key protein residues (yellow sticks). (**i**) Examples of virtual hits from the receptor-based virtual screen in **g**.

shapes that matched those of the ligands 6-FP (**Fig. 1e**) and 5-OP-RU (**Supplementary Fig. 1a**); this led to 16 'virtual hits', including those presented here (**Fig. 1f**). A third *in silico* approach involved receptor-based virtual docking (**Fig. 1g**) of a subset of 470 of the 1,216 FDA-approved drugs (molecular size, 150–300 Da) into the ternary crystal structure of 5-OP-RU bound to a complex of MR1 and a MAIT TCR (**Fig. 1h** and **Supplementary Fig. 1b**). This led to identification of 20 virtual hits, including those presented here (**Fig. 1i**). In summary, these parallel approaches (**Fig. 1**) produced 183 distinct hits with chemically diverse structures (**Supplementary Tables 1** and **2**), among which 22 were identified as previously unknown modulators of the MR1–MAIT cell axis (**Supplementary Fig. 1c**); this suggested that MR1 has the potential to bind to many structurally different compounds.

Inhibition or activation of MAIT cells by diverse MR1 ligands

Through the use of *in vitro* functional assays, we evaluated 81 of the *in silico* hits identified above for their ability to bind to MR1 and to stimulate MAIT cells. The MR1-binding and cell-stimulatory ability of the compounds were assessed in experiments in which an antigen-presenting cell line (C1R human lymphoblastoid cells) overexpressing MR1 (C1R.MR1 cells) and a T cell line (Jurkat human T lymphocytes) overexpressing the A-F7 MAIT TCR that uses TRBV6-1 (Jurkat.MAIT-A-F7 cells) were incubated together, along with the test compound. Approximately one quarter of the compounds, including nine drugs, five flavones and eight small-molecule compounds, had a measurable effect on the upregulation of the surface expression of MR1 and/or the stimulation of MAIT cells (**Fig. 2a**,

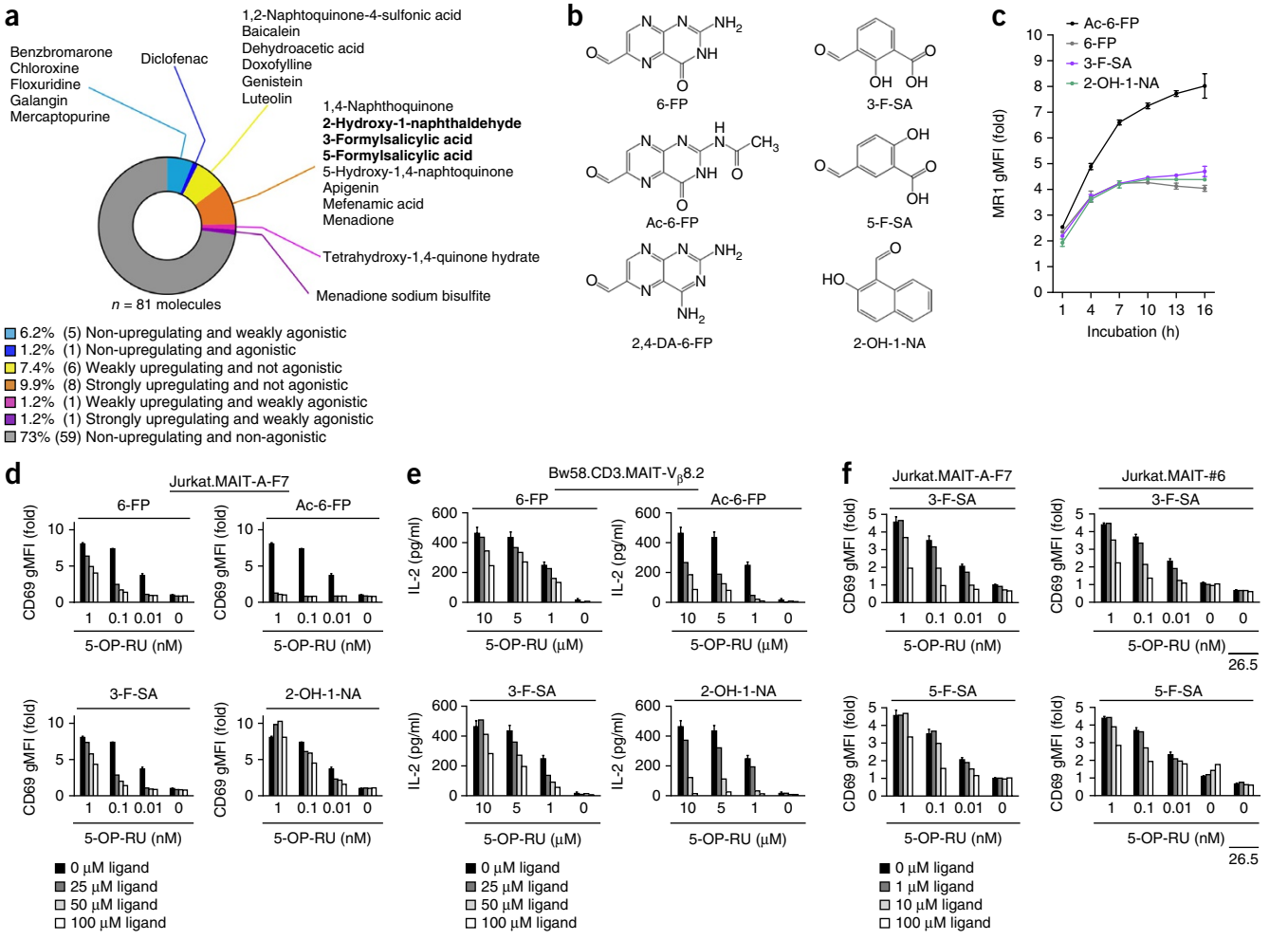

Figure 2 Drugs and drug-related molecules cause upregulation of the cell-surface expression of MR1 and inhibition of MAIT cells. (**a**) Ability of drugs and drug-related molecules (bold indicates ligands of interest) to upregulate MR1 expression on the surface of C1R.MR1 cells or to activate Jurkat.MAIT-A-F7 cells (agonistic) (key), assessed in a functional screen (normalized results in a combined assay, **Supplementary Table 3**); results (key) indicate proportion among the 81 molecules assessed (percent value) or total number in group (in parentheses). (**b**) Chemical structures of the MR1 ligands 6-FP, Ac-6-FP, 2,4-DA-6-FP, 3-F-SA, 5-F-SA and 2-OH-1-NA (labels below structure). (**c**) Surface expression of MR1 by C1R.MR1 cells over time in the presence of 100 μM Ac-6-FP, 6-FP, 3-F-SA or 2-OH-1-NA (key); results are presented as the geometric mean fluorescence intensity (gMFI), 26.5-fold of the background intensity. (**d**) Activation of Jurkat.MAIT-A-F7 cells by various concentrations of 5-OP-RU (horizontal axis) in the presence of C1R.MR1 cells and various concentrations (key) of the ligands 6-FP, Ac-6-FP, 3-F-SA or 2-OH-1-NA (above plots), assayed by flow cytometry analyzing CD69 staining and presented relative to background intensity. (**e**) Activation of Bw58.CD3.MAIT-Vβ8.2 cells by 5-OP-RU in the presence of M12.C3 cells transduced with mouse MR1 and various concentrations (key) of the ligands 6-FP, Ac-6-FP, 3-F-SA or 2-OH-1-NA (above plots), as assessed by IL-2 production. (**f**) Activation of Jurkat.MAIT-A-F7 cells (left) and Jurkat.MAIT-#6 cells (right) by various concentrations of 5-OP-RU (horizontal axis) in the presence of C1R.MR1 cells and various concentrations (key) of the ligands 3-F-SA or 5-F-SA (above plots), assessed as in **d**; far right includes blockade of MR1 by monoclonal antibody 26.5 (below plot). Data are representative of one experiment (**a**) or are from one experiment representative of three experiments (**c**–**f**; mean + s.e.m. of technical triplicates).

Supplementary Table 3 and **Supplementary Figs. 1c** and **2a**). Of the sixteen compounds that upregulated MR1 expression, eight were agonists (**Fig. 2a** and **Supplementary Fig. 2a**). Thus, although MR1 was able to bind diverse chemical ligands (**Supplementary Fig. 1c**), the requirements related to the activation of MAIT cells were more stringent. Notably, many of the aromatic aldehydes, ketones or carboxylic acids that fit into MR1 (**Fig. 1a** and **Supplementary Tables 1–3**) did not upregulate the cell-surface expression of MR1 appreciably (**Fig. 2a**, **Supplementary Table 3** and **Supplementary Figs. 1c** and **2a**), which indicated that simply neutralizing the charge of Lys43 (MR1) through either Schiff-base formation or an ionic interaction was insufficient for binding to MR1.

We then compared the MR1-binding and inhibitory ability of 6-FP and acetyl-6-formylpterin (Ac-6-FP) with that of a selection of the compounds that strongly upregulated MR1 expression but were not agonists. These included 3-formylsalicylic acid (3-F-SA), 5-formylsalicylic acid (5-F-SA) and 2-hydroxy-1-naphthaldehyde (2-OH-1-NA) (**Fig. 2b**). The kinetics and extent of upregulation of MR1 expression of these three compounds were similar to those of 6-FP (**Fig. 2c** and **Supplementary Fig. 2b**). 3-F-SA and 2-OH-1-NA also effectively inhibited the activation of MAIT cells in the presence of 5-OP-RU in a dose-dependent manner, as determined by measurement of expression of the activation marker CD69 on three Jurkat cell lines expressing MAIT TCRs: Jurkat.MAIT-A-F7 cells (defined above), Jurkat.MAIT-#6 cells (expressing a TCR that uses TRBV6-4) and Jurkat.MAIT-C-F7 cells (expressing a TCR that uses TRBV20) (**Fig. 2d** and **Supplementary Fig. 2c**). As determined by the half-maximum inhibitory concentration across the range of 5-OP-RU doses tested, we established that Ac-6-FP was the most potent inhibitor, followed by 3-F-SA and 6-FP, which were comparable in their ability to inhibit the activation of MAIT cells, with 2-OH-1-NA being the least potent inhibitor (**Supplementary Table 4**). A similar pattern was observed for production of the cytokine IL-2 (as a marker of activation) by a mouse BW58 cell line transduced to express a MAIT TCR (BW58.CD3.MAIT-Vβ8.2 cells) when those cells were incubated with a mouse M12.C3 B lymphocyte cell line transduced with mouse MR1, as an antigen-presenting cell (**Fig. 2e** and **Supplementary Table 4**). Upregulation of CD69 expression or IL-2 production by the T cell lines in response to stimulation with phorbol-12-myristate-13-acetate plus ionomycin was not impaired in the presence of these inhibitors (**Supplementary Fig. 2c**,**d**); similarly, stimulation of a conventional T cell line by its cognate antigen was not impaired (**Supplementary Fig. 2e**), which indicated that the inhibitory effects were specific to the MR1–MAIT cell axis.

The fine specificity underpinning the activation and inhibition of Jurkat cells expressing MAIT TCRs by chemically similar structures was evident in a comparison of 3-F-SA and 5-F-SA. Although 3-F-SA did not stimulate any of the three MAIT-TCR-expressing Jurkat cell lines, 5-F-SA showed modest activation of Jurkat.MAIT-#6 cells that was blocked by a monoclonal antibody (26.5) to MR1, but 5-F-SA did not activate Jurkat.MAIT-A-F7 cells (**Fig. 2f**) or Jurkat.MAIT-C-F7 cells (data not shown). This indicated that the use of TCR β-chains by MAIT cells was able to 'fine tune' the responsiveness to certain ligands.

Binding and upregulation of MR1 by a drug degradation product

The folic-acid derivatives aminopterin and methotrexate have been used to treat certain cancers and autoimmune disorders, including rheumatoid arthritis and psoriasis[20]. Aminopterin readily photodegrades in ultraviolet light to form 2,4-diamino-6-formylpteridine (2,4-DA-6-FP). Although methotrexate is more stable, it nevertheless forms the same photodegradation product[21]. Given the similarity between the naturally occurring photodegradation products 6-FP and 2,4-DA-6-FP (**Supplementary Fig. 3a**), we reasoned that 2,4-DA-6-FP might also upregulate the cell-surface expression of MR1. Indeed, photodegradation preparations of aminopterin supported the refolding of MR1 and upregulated the cell-surface expression of MR1, whereas untreated aminopterin did not (**Supplementary Fig. 3b–d**). Mass spectrometry comparing the captured antigen with the synthetically produced compound showed that 2,4-DA-6-FP was captured within the refolded MR1 molecule (**Supplementary Fig. 3e**). Collectively, these studies identified the metabolite 2,4-DA-6-FP as a previously undescribed ligand of MR1.

Activation of MAIT cells by diclofenac metabolites

We also characterized an agonist drug identified by the functional screen: diclofenac (DCF). Although it did not apparently upregulate cell-surface expression of MR1, DCF activated Jurkat.MAIT-A-F7 cells, with this activation being blocked by the monoclonal antibody 26.5 to MR1 and competitively inhibited by Ac-6-FP in a dose-dependent manner (**Fig. 3a**). The level of stimulation by DCF at a ligand concentration of 100 μM was greater than that of the ribityllumazine agonists, 6,7-dimethyl-8-D-ribityllumazine (RL-6,7-DiMe) and 7-hydroxy-6-methyl-8-D-ribityllumazine (RL-6-Me-7-OH)[16] and was comparable to maximum stimulation with 5-OP-RU, albeit with 5-OP-RU at a much lower concentration (**Fig. 3a**). Although DCF activated Jurkat.MAIT-A-F7 cells, which express a TCR that uses TRBV6-1, it did not activate the two other cell lines, Jurkat.MAIT-#6, and Jurkat.MAIT-C-F7, which express TCRs that use TRBV6-4 or TRBV20, respectively (**Fig. 3b**); this indicated that the agonistic properties of DCF were dependent on the TCR β-chain segment used,

Figure 3 DCF metabolites activate MAIT cell lines in an MR1-dependent manner. (**a**) Activation of Jurkat.MAIT-A-F7 cells by various concentrations (horizontal axis) of 5-OP-RU or DCF in the presence (26.5) or absence of monoclonal antibody 26.5 to MR1 (below plot), or by various concentrations of RL-6-Me-7-OH or RL-6,7-DiMe, or Ac-6-FP in the presence (DCF) or absence of 100 μM DCF (below plot), assessed as IL-2 production and presented as absorbance at 492 nm (A_{492}). (**b**) Activation of Jurkat.MAIT-A-F7, Jurkat.MAIT-#6 or Jurkat.MAIT-CF7 cells (key) by various concentrations (horizontal axis) of 5-OP-RU, RL-6,7-DiMe, RL-6-Me-7-OH or DCF (assessed and presented as in **Fig. 2d**). (**c**) Activation of Jurkat.MAIT-A-F7, Jurkat.MAIT-#6 or Jurkat.MAIT-C-F7 (above plots) cells by various concentrations (horizontal axis) of DCF or Ac-6-FP or neither (–) in the presence of various concentrations (key) of 5-OP-RU (assessed and presented as in **Fig. 2d**). (**d**) Activation of Jurkat.MAIT-A-F7 cells (left) and Jurkat.MAIT-#6 cells (right) by various concentrations (horizontal axis) of 5-OP-RU, 6-FP or Ac-6-FP, or DCF or its metabolites (key), without or with Ac-6-FP or monoclonal antibody 26.5 (below plot, right end), in the presence of C1R.MR1 cells, or by no ligand (–) or phorbol-12-myristate-13-acetate plus ionomycin (PMA + iono) in the absence of C1R.MR1 cells (assessed and presented as in **Fig. 2d**). ND, not determined. (**e**) Chemical structures of DCF, 4′-OH-DCF, 5-OH-DCF, 4′,5-diOH-DCF, DCF acyl-β-D-glucuronide allyl ester or DCF acyl-β-D-glucuronide (counterclockwise from top left). (**f**) Extracted-ion chromatograms (Q1–Q3 transition) of the surface-isolated ligands (red) and chemically synthesized ligands (black) Ac-6-FP, 3-F-SA, 5-OH-DCF and 4′,5-diOH-DCF (above plots), as well as 4′-OH-DCF (gray) (top row), and enhanced product ion spectra of the ligands Ac-6-FP, 3-F-SA, 5-OH-DCF and 4′,5-diOH-DCF that immunoprecipitated together with MR1 from the surface of C1R.MR1 cells (bottom row). Data are from one experiment representative of three independent experiments (**a**,**b**,**f**; mean + s.e.m. of technical triplicates) or one experiment representative of two experiments (**c**,**d**; mean + s.e.m. of technical triplicates).

suggestive of activation specific to the subset of MAIT cell. Moreover, the activation of Jurkat.MAIT-A-F7 cells by 5-OP-RU was increased in the presence of DCF, and DCF did not inhibit the activation of Jurkat.MAIT-#6 cells or Jurkat.MAIT-C-F7 cells by 5-OP-RU (**Fig. 3c**).

To determine if DCF was broadly stimulatory to MAIT cells, we tested a panel of 12 cell lines that express MR1-restricted TCRs[13,22] that varied in their use of TCR α- and β-chains, as well as in their reactivity to 5-OP-RU, 6-FP, Ac-6-FP and an absence of ligand, by assessing their reactivity to DCF in the presence of C1R.MR1 cells (**Fig. 3d** and **Supplementary Fig. 4a**,**b**). Given that DCF is known to be metabolized, we determined whether the observed stimulation was due to DCF itself or to any (or all) three of its hydroxyl metabolites

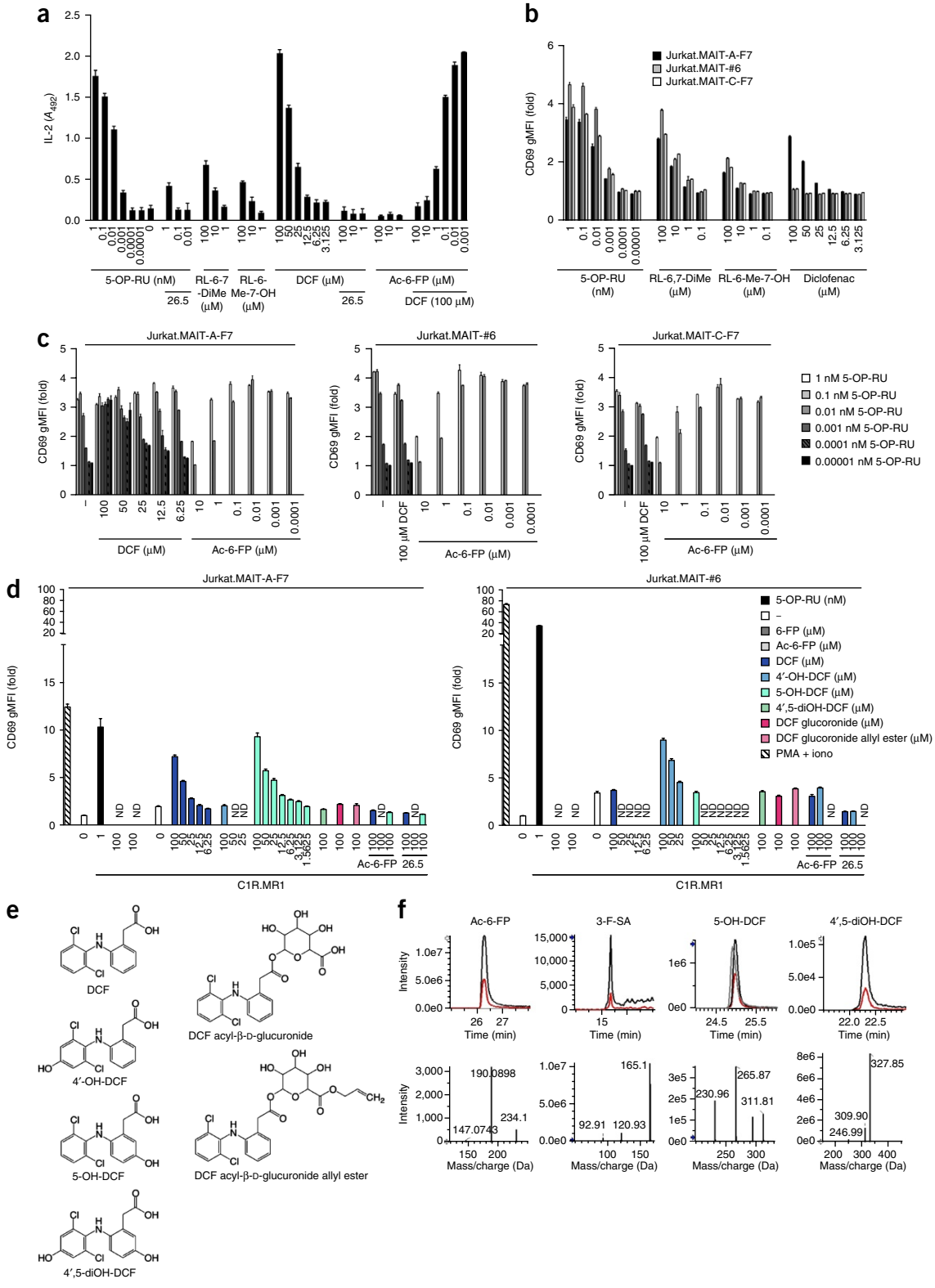

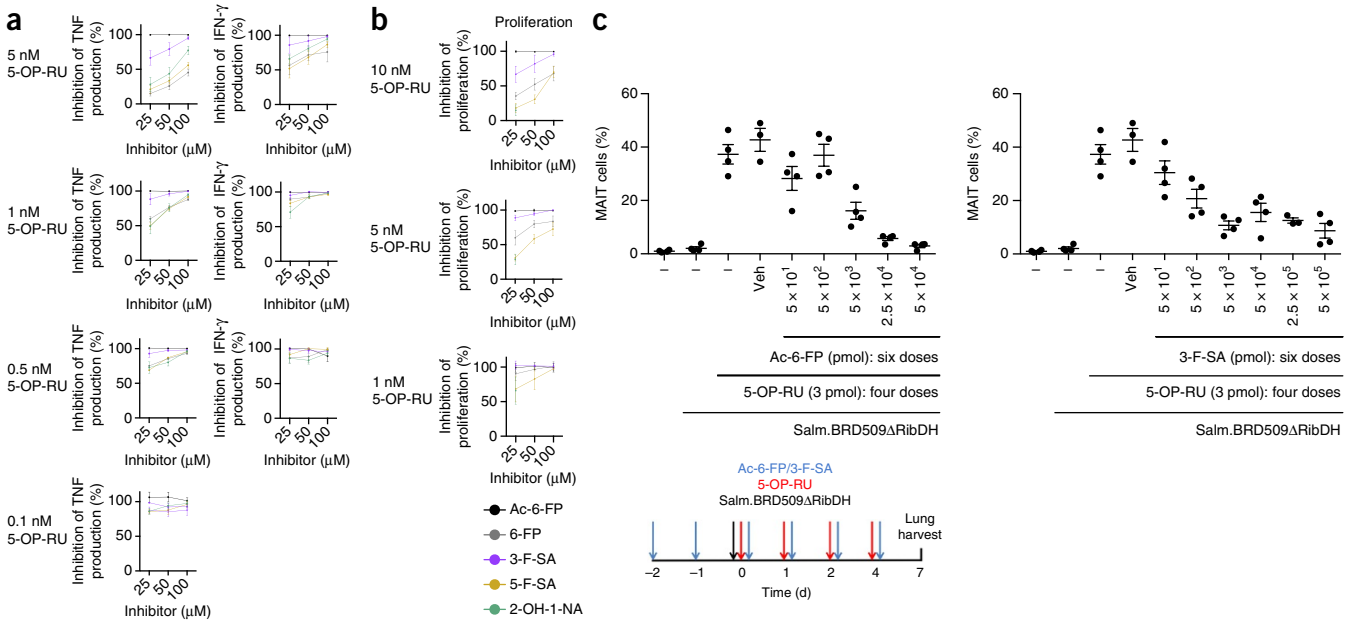

Figure 4 Drugs and drug-related molecules inhibit the activation of MAIT cells *ex vivo* and *in vivo*. (**a**,**b**) Inhibition of the production of TNF (left) or IFN-γ (right) (**a**) or the proliferation (**b**) of human MAIT cells (live, CD3$^+$TRAV1-2$^+$ and positive for the MR1–5-OP-RU tetramer) *ex vivo* in cultures of monocyte-derived DCs incubated together with peripheral blood mononuclear cells (depleted of autologous monocytes) in the presence of various concentrations of 5-OP-RU (left margin) and various doses (horizontal axes) of inhibitory ligands (key); for 2-OH-1-NA, the proliferative response could be determined only at a concentration of 25 μM, higher concentrations impaired the ability to be activated by stimulation with plate bound anti-CD3 plus anti-CD28 (data not shown). (**c**) Accumulation of MAIT cells in the lungs of C57BL/6 mice given intranasal administration of vehicle (Veh) or various concentrations (horizontal axis) of Ac-6-FP (left) or 3-F-SA (right) (below plot) and left unstimulated (–) or stimulated by intranasal administration of 5-OP-RU and Salm.BRD509Δ*ribDH* (below plot); results are presented as the frequency among αβ T cells. Each symbol represents an individual mouse ($n = 4$ (or $n = 3$ if one was excluded due to technical issues)); small horizontal lines indicate the mean (±s.e.m.). Data are representative of one experiment per donor (**a**,**b**; mean ± s.e.m. of $n = 5$ donors; results pooled) or are from one experiment representative of three experiments with similar results (**c**).

(4′-hydroxy DCF (4′-OH-DCF), 5-hydroxy DCF (5-OH-DCF) and 4′,5-dihydroxy DCF (4′,5-diOH-DCF)) and two glucuronide conjugates (DCF acyl-β-D-glucuronide and DCF acyl-β-D-glucuronide allyl ester) (**Fig. 3e**). DCF and its metabolites did not modulate the stimulation of a conventional T cell line by its cognate antigen (**Supplementary Fig. 4b**), which ensured the specificity of the responses observed. Of the cell lines tested, the Jurkat.MAIT-A-F7 cell line (and thus the A-F7 TCR) was specifically stimulated by DCF; indeed, for this cell line, stimulation by 5-OH-DCF was stronger than stimulation by DCF itself (**Fig. 3d**,**e**). Similarly, another 10 of the 12 cell lines tested responded modestly to 4′-OH-DCF, whereas none of the other DCF metabolites yielded specifically increased responses (**Fig. 3d**,**e** and **Supplementary Fig. 4a**,**b**). Collectively, these results indicated that the observed activation of a MAIT cell line by DCF might be more attributable to one of its metabolites.

Presentation of drugs and drug-like molecules by MR1

Given that many drugs are metabolized within cells, we next sought to determine whether some of the compounds that inhibited or activated MAIT cells had been metabolized in antigen-presenting cells before being presented by MR1 at the cell surface. To investigate this, we immunoprecipitated MR1 from the surface of C1R.MR1 cells and used mass spectrometry to analyze the ligands captured by MR1. To validate this approach, we incubated C1R.MR1 cells with Ac-6-FP and specifically detected this ligand in the MR1 eluate fraction (**Fig. 3f**). Using this approach, we also determined that 3-F-SA was presented by MR1 on the cell surface (**Fig. 3f**). Next, we established that it was DCF metabolites, not DCF itself, that were presented on the cell surface: the metabolites of DCF that bound to MR1 on the cell surface included hydroxylated DCF (either 5-OH-DCF or 4′-OH-DCF (which are indistinguishable via mass spectrometry), or a combination of the two) and 4′,5-diOH-DCF, a result subsequently confirmed by mass spectrometry of the pure, chemically synthesized DCF metabolites (**Fig. 3f**). DCF and the glucuronated species were not detected (data not shown), which could have been due to cell-type-specific metabolism or the larger size of glucuronated DCF that no longer fits the ligand-binding pocket of MR1. Thus, drugs and drug-like molecules, as well as their metabolites, were presented by MR1 to MAIT cells.

Ex vivo modulation of the activity of MAIT cells

Next we established the extent to which three of those newly identified MR1 ligands (3-F-SA, 5-F-SA and 2-OH-1-NA, and the controls 6-FP and Ac-6-FP) were able to modulate the activity of MAIT cells *ex vivo*. We obtained peripheral blood mononuclear cells from five donors and identified MAIT cells as TRAV1-2$^+$ lymphocytes positive for the MR1–5-OP-RU tetramer, among the CD3$^+$ population of cells. We then assessed competitive inhibition by the drugs and drug-like molecules of the 5-OP-RU–dependent activation of the MAIT cells, assaying production of the inflammatory cytokines TNF and IFN-γ as activation markers. The compounds inhibited the activation of MAIT cells in a dose-dependent manner, with Ac-6-FP as the most potent competitive inhibitor, followed by 3-F-SA (**Fig. 4a**). Less-potent inhibitory effects were observed for 2-OH-1-NA, 5-F-SA and 6-FP (**Fig. 4a**). We also assessed the ability of these compounds to inhibit the proliferation of MAIT cells when incubated with 5-OP-RU. The pattern of inhibitory effects on cytokine production mirrored

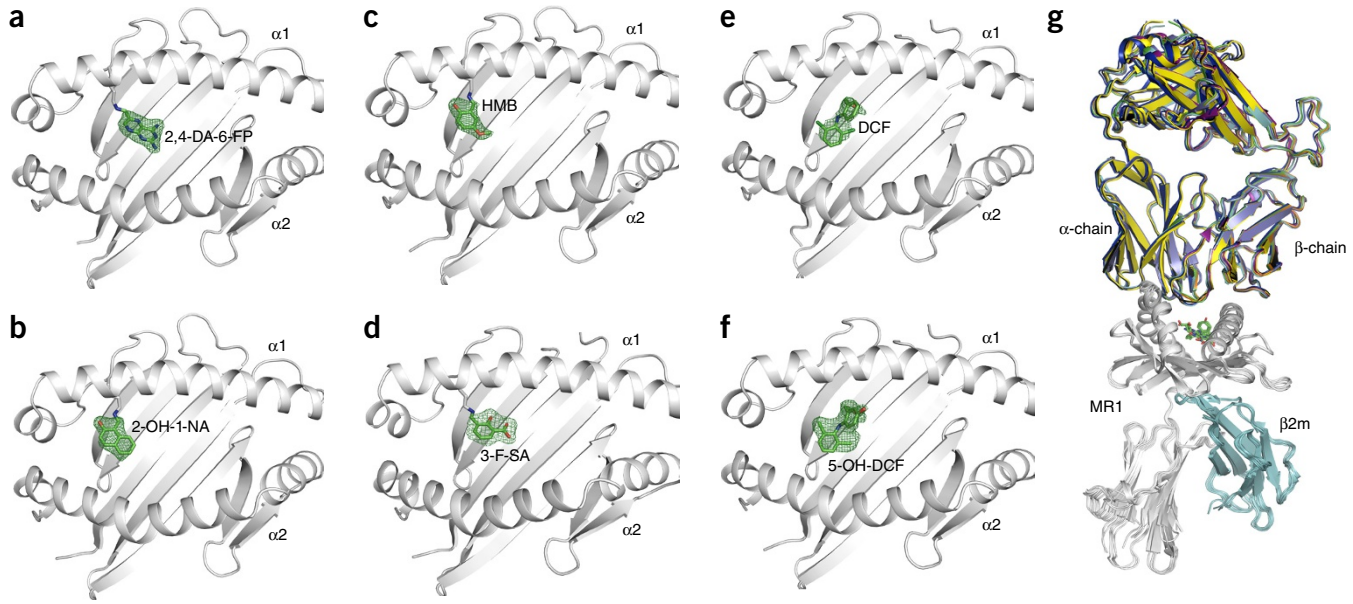

Figure 5 MR1 structures with drugs and drug-related molecules. (**a**–**f**) Omit maps of 2,4-DA-6-FP (**a**), 2-OH-1-NA (**b**), HMB (**c**), 3-F-SA (**d**), DCF (**e**) and 5-OH-DCF (**f**) after simulated-annealing refinement (with the Phenix-refine crystallographic structure-refinement program), presented as an $F_o - F_c$ map (observed structure factor – calculated structure factor; green mesh) contoured at 3σ. (**g**) Overlay of all drug and drug-related ternary structures. β2m, β_2-microglobulin.

the inhibitory effects on cell proliferation (**Fig. 4b**). MAIT cells and TRAV1-2$^+$ cells negative for the MR1–5-OP-RU tetramer (non-MAIT cells) produced cytokines in response to stimulation with phorbol-12-myristate-13-acetate plus ionomycin (**Supplementary Fig. 5a**) and proliferated in response to plate-bound antibody to the TCR invariant chain CD3 (anti-CD3) and antibody to the costimulatory receptor CD28 (anti-CD28) (**Supplementary Fig. 5b**), regardless of the presence of inhibitory molecules, which indicated that toxicity was unlikely to have stimulated inhibition. Thus, drugs and drug-like molecules affected the activity of MAIT cells *ex vivo*.

In vivo modulation of the activity of MAIT cells

We next established the efficacy of two of those ligands in inhibiting the proliferation of MAIT cells *in vivo*; for this, we used a previously established MAIT cell model in C57BL/6 mice[23]. In this model, synthetic 5-OP-RU in conjunction with stimulation via Toll-like receptors (TLRs) causes MAIT cells to accumulate in the lungs to make up to about 25–50% of αβ T cells, compared with their abundance of 0.5–2% in the lungs of naive mice. TLR stimulation can be provided either by synthetic TLR agonists such as the synthetic lipopeptide Pam_2Cys (which triggers TLR2 and TLR6)[24], the synthetic RNA duplex poly(I:C) (which triggers TLR3) or CpG dinucleotides (which trigger TLR9) or by bacteria deficient in the riboflavin pathway, as we demonstrated for the live attenuated vaccine strain of *Salmonella enterica* serovar Typhimurium (*S.* Typhimurium BRD509) that is deficient in riboflavin synthesis (Salm.BRD509Δ*ribDH*) (data not shown).

In a model mimicking infection, in which 5-OP-RU is supplied extracellularly for antigen presentation in conjunction with stimulation of the TLRs by the intracellular bacteria Salm.BRD509Δ*ribDH*, repeated application of Ac-6-FP or 3-F-SA inhibited the accumulation of MAIT cells in the lungs in a dose-dependent manner (**Fig. 4c**). Notably Ac-6-FP or 3-F-SA had no effect on the abundance of bacterial colony-forming units, the absolute number of non-MAIT αβ T cells or IL-17 production by non-MAIT αβ T cells in the lungs in response to Salm.BRD509Δ*ribDH* (**Supplementary Fig. 6a**,**b**), which indicated that the inhibitory effects were not due to toxic effects of the inhibitors on the bacteria or T cells. Thus, these inhibitors were able to effectively abolish the activation of MAIT cells *in vivo*.

Structures of MAIT TCR–MR1–ligand complexes

Next we determined the crystal structures for the A-F7 MAIT TCR (which uses TRBV6-1) bound to MR1 presenting non-stimulatory ligands (2,4-DA-6-FP, 2-hydroxy-5-methoxybenzaldehyde (HMB), 2-OH-1-NA and 3-F-SA) and two activating ligands (DCF and 5-OH-DCF) (**Supplementary Table 5**). All drugs and drug-related compounds were clearly visible within the antigen-binding cleft of MR1 (**Fig. 5a**–**f**). The MAIT TCR docked atop the six MR1–drug or MR1–drug-like compound complexes with very similar topology (**Fig. 5g**, **Supplementary Fig. 7a**–**h** and **Supplementary Table 6**). Thus, the recognition of diverse chemical scaffolds did not translate into diverse docking of the MAIT TCR on MR1. Further, all of the drugs and drug-like molecules were located within the A′-pocket of MR1 (**Figs. 5**–**7**), which not only validated the results of the *in silico* approaches (**Fig. 1**) but formally demonstrated that this pocket was sufficiently versatile to accommodate distinct chemical identities. Furthermore, the high-resolution structural information allowed thorough examination of the amino acids in MR1 that were responsible for ligand capture. All of these non-stimulatory ligands formed a Schiff base with Lys43 at the base of the aromatic cradle and, consistent with their non-stimulatory properties, none of them directly contacted the MAIT TCR (**Fig. 6a**–**e**). 2,4-DA-6-FP was located in a position essentially identical to that of 6-FP, in which the pteridine ring of 2,4-DA-6-FP was sandwiched between Tyr7 and Trp69 and formed additional aromatic pi-interactions with Trp156 and Tyr62 while abutting Ile96 of MR1 (**Fig. 6a**,**b**). The difference between 6-FP and 2,4-DA-6-FP is the presence of a carbonyl group in the former versus an amino group in the latter at position 4 of the pteridine ring. This difference affected the base of the cleft, with either the carbonyl or amino group nestling against Arg9 in the MR1–6-FP complex (**Fig. 6a**,**b**). That last interaction is unfavorable and probably accounted for the weaker upregulation

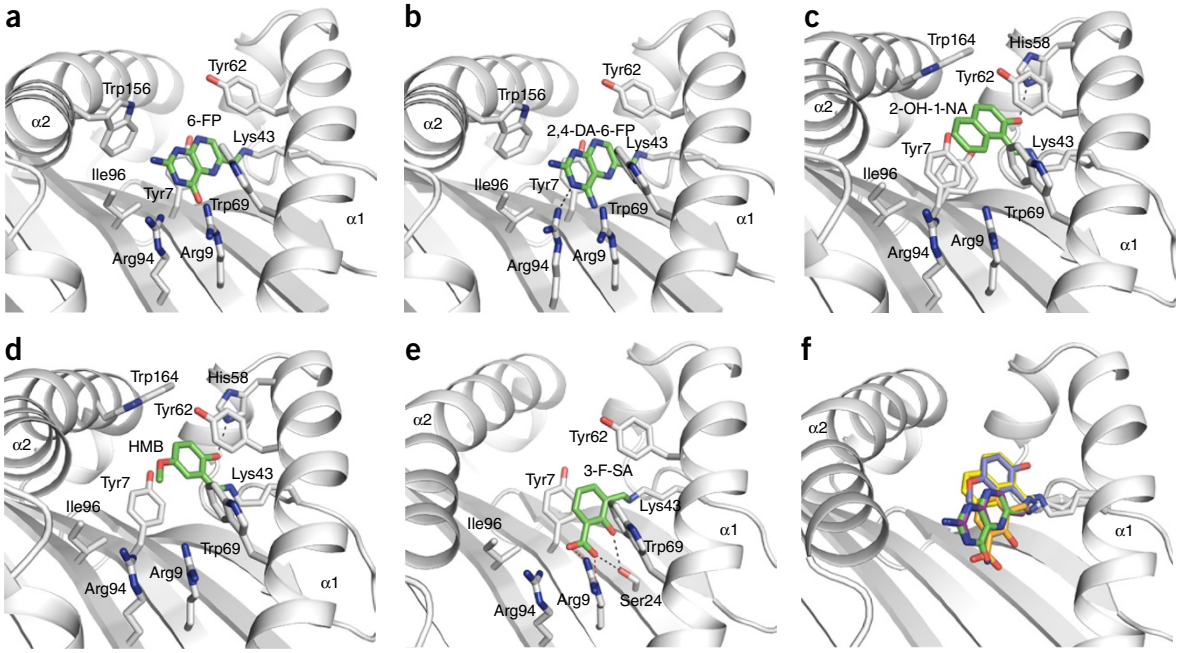

Figure 6 Inhibitors bound within the MR1 cleft. (**a**–**e**) Structures showing MR1 residues (white) that directly contact 6-FP (**a**), 2,4-DA-6-FP (**b**), 2-OH-1-NA (**c**), HMB (**d**) or 3-F-SA (**e**) (green): black dashed lines, hydrogen bonds; red dashed lines, salt bridges. (**f**) Superposition of 6-FP (green), 2,4-DA-6-FP (purple), 2-OH-1-NA (yellow), HMB (slate) and 3-F-SA (orange) within the binding cleft of MR1.

of the cell-surface expression of MR1 (**Supplementary Fig. 3b**,**c**). Thus, subtle chemical differences between ligands were able to affect the associated MR1-binding properties.

The compound 2-OH-1-NA, like 6-FP, has a bicyclic ring structure, and while the planes of the aromatic rings were similarly disposed, 2-OH-1-NA was displaced by ~4Å toward the α1-helix of MR1 (**Fig. 6c**). In adopting this binding mode, its 2-hydroxy group, the only polar moiety of 2-OH-1-NA, formed a hydrogen bond to His58 and packed against Trp164 of MR1, while the interactions with Arg9, Arg94 and Trp69 were lost (**Fig. 6c**). 3-F-SA and HMB are monocyclic (**Fig. 6d**,**e**); the latter compound was directly superposable over 2-OH-1-NA and thereby mediated similar interactions with MR1, including the hydrogen bond with His58 (**Fig. 6d**–**f**). The 5-methoxy group was not involved in polar interactions but was stabilized by packing against Tyr7 of MR1 (**Fig. 6d**). In contrast, 3-F-SA was rotated in the same plane by approximately 70° around the Schiff base relative to the positioning of 2-OH-1-NA and, accordingly, was accommodated in a different region of the A′-pocket of MR1 (**Fig. 6e**). Specifically, the carboxyl group of 3-F-SA was oriented to form a salt bridge with Arg9 and hydrogen bond to Ser24, while its aromatic ring was wedged between Tyr7 and Trp69 of MR1 (**Fig. 6e**). These additional interactions were consistent with the finding that 3-F-SA represented a potent inhibitor of the function of MAIT cells (**Fig. 2c**). Thus, there was sufficient plasticity within the A′-pocket of MR1 to accommodate diverse chemical scaffolds.

MAIT TCR–MR1–stimulatory ligand complexes

Comparison of the crystal structures of the MAIT TCR bound to MR1 presenting DCF or 5-OH-DCF provided insight into the agonistic properties of 5-OH-DCF (**Fig. 7** and **Supplementary Tables 7** and **8**). Neither species formed a Schiff base with MR1 (**Fig. 7d**,**e**), consistent with the poor ability of DCF (and metabolites thereof) to upregulate MR1 expression (**Supplementary Table 3** and data not shown) and reminiscent of results obtained for the weak agonist RL-6-Me-7-OH[17]. Despite that, the positioning of Lys43 remained relatively well fixed within the MR1 cleft, and it formed a hydrogen bond with the adjacent residue His58 (**Fig. 7d**,**e**). In contrast to the non-stimulatory compounds, DCF directly contacted the MAIT TCR (**Fig. 7d**). However, the mode for the binding of DCF within the cleft and the subsequent contacts of DCF and MR1 with the MAIT TCR were markedly different from the binding modes and contacts of the MAIT TCR–MR1–5-OP-RU interactions (**Fig. 7c**–**e**). The plane of the central phenylacetic acid ring of DCF was essentially perpendicular to that of 5-OP-RU and all other MR1-ligand complexes (**Fig. 7c**–**f**). Moreover, the dichlorophenyl and phenylacetic acid rings were positioned approximately orthogonal to each other (**Fig. 7a**). Here, the dichlorophenyl group was buried toward the base of the cleft, wedged among MR1 residues Tyr7, Tyr62, Trp156 and Trp164 (**Fig. 7a**). One of the chloro groups pointed toward Arg94, whereas the other was shielded by Tyr62 and Trp164 and formed a halogen bond with Lys43 (**Fig. 7a**). The phenylacetic acid group was sandwiched between Arg9 and Tyr62, with the acetic acid moiety salt-bridging to Arg9 and forming a hydrogen bond with Ser24 of MR1 (**Fig. 7a**). Notably, to accommodate the dichlorophenyl ring of DCF within the cleft, MR1 underwent some conformational changes, including a slight reorientation of Tyr7 and, most notably, flipping of Trp69 out of the way to avoid steric clashes with the ligand (**Fig. 7c**,**d**). The reconfiguration of Trp69 had a 'knock-on' effect, in that it caused remodeling of the CDR3β loop of the MAIT TCR, with the TCR residue Glu99β swinging down to salt bridge with MR1 residues Arg9 and Arg94, while Trp96β of the TCR re-orientated to form new contacts with Met72 and Trp69 of MR1 (**Fig. 7c**,**d**). The hydroxyl moiety of Tyr95α from the TCR CDR3α loop had a pivotal role in interacting with the ribityl chain of 5-OP-RU (**Fig. 7c**) but did not mediate polar interactions with DCF (**Fig. 7d**). Instead, the Tyr95α aromatic ring stacked against the phenylacetic acid ring, and the latter also formed van der Waals contacts with Glu99β from the CDR3β loop (**Fig. 7d**). The mode of binding of DCF was very similar to that of 5-OH DCF, with one

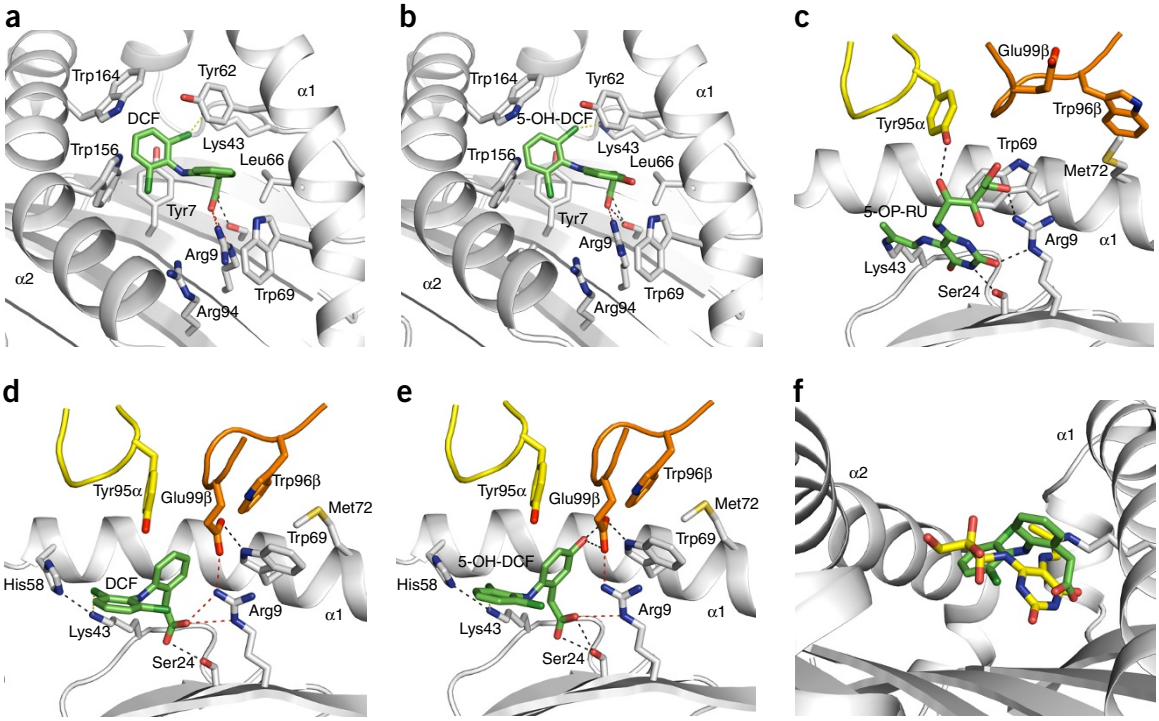

Figure 7 Complexes of MR1–MAIT TCR with DCF and a specific metabolite. (**a**,**b**) Structures showing MR1 residues (white) that directly contact DCF (**a**) or 5-OH-DCF (**b**) (green): black dashed lines, hydrogen bonds; red dashed lines, salt bridges; yellow dashed lines, halogen bonds. (**c**–**e**) Interactions between the CDR3α loop (yellow) and CDR3β loop (orange) of the A-F7 MAIT TCR, with MR1 presenting 5-OP-RU (**c**), DCF (**d**) or 5-OH-DCF (**e**) (colors and labels as in **a**,**b**). (**f**) Superimposition of 5-OP-RU (yellow) and DCF (green) bound within MR1.

notable difference: the 5-OH group of 5-OH-DCF formed a hydrogen bond with Glu99β from the CDR3β loop, and this additional contact to the TCR correlated with its agonist properties and with its ability to stimulate a specific MAIT TCR (**Fig. 7e**).

DISCUSSION

A central question in the biology of MAIT cells is whether MR1 is able to present ligands distinct from riboflavin precursors and folic acid-derived metabolites. Here we found that MR1 was able to present a heterogeneous array of organic compounds with diverse chemical scaffolds, including some commonly prescribed therapeutics, that were able to modulate the activity of MAIT cells. Given that pyrimidines are widely used scaffolds in therapeutics, we hypothesized that MR1 might present drugs and drug-like molecules. Indeed, the MR1-binding compounds identified here included a wide range of drugs and drug-like molecules, fragments and derivatives. Our findings also have implications for any future therapy based on the inhibition of MAIT cells, as we demonstrated that administration of MR1-inhibitory ligands affected the function of MAIT cells in an *in vivo* setting. Our work also suggested that if endogenous ligands have similar chemical scaffolds, they may also affect the function of MAIT cells.

Of the ligands that upregulated cell-surface expression of MR1 to detectable levels, all formed a Schiff base with MR1, which emphasizes the importance of forming a covalent adduct[25]. Moreover, the various non-stimulatory ligands adopted different conformations and contacts within the A′-pocket of MR1, which also correlated with differences in their ability to upregulate MR1 expression on the cell surface and inhibit the activation of MAIT cells. Notably, while 3-F-SA was non-stimulatory for the MAIT TCRs tested, 5-F-SA weakly activated a cell line expressing a MAIT TCR. This resonates with the finding that diversity in the MAIT TCR repertoire can permit some folic acid derivatives to stimulate some MR1-restricted T cells and MAIT cells[22].

Of the drugs tested that activated MAIT cells, DCF showed the greatest potency. Its stimulatory activity was traced to naturally occurring DCF metabolites presented by MR1 on the cell surface. The mode of binding of DCF within the MR1 cleft was distinct from that of other MR1-bound ligands, as it did not form a Schiff base with Lys43, as has also been observed for some ribityllumazines[17]. The 5-OH-DCF metabolite directly contacted the α- and β-chains of the MAIT TCR, which provided insight into both its antigenicity and the ability of the DCF metabolite 4′-OH-DCF to activate specific MAIT TCRs[22], suggestive of the activation of specific subsets of MAIT cells by DCF metabolites.

A notable consideration is whether the drugs that modulated the activity of MAIT cells manifest clinically important side effects. Although the degree to which methotrexate and aminopterin degrade into 2,4-DA-6-FP in patients is unclear, chemotherapeutic administration of a high dose of methotrexate can result in much higher plasma concentrations of the drug than those required to upregulate MR1 expression on the cell surface[26,27]. Our results obtained for DCF might potentially reconcile reported immunological complications, such as severe hepatotoxicity. Indeed, DCF was able to activate a MAIT TCR at a concentration that can be achieved in patients after an oral dose[28]. Interestingly, pharmacogenetic studies have revealed that the hepatotoxicity of DCF is much more prevalent in patients with polymorphisms in the enzymes responsible for DCF catabolism, including CYP2C8, which is responsible for conversion of DCF into 5-OH-DCF[29].

This is the first description, to our knowledge, of drugs affecting the function of MR1, a monomorphic antigen-presenting molecule. Unlike HLA-linked drug hypersensitivities, in which a drug can exert

its effect by altering the repertoire of peptides bound by the HLA allomorph[30], the more constricted nature of the MR1 binding pocket limits binding to either the drug or a ligand associated with vitamin-B2 synthesis, but not both. Some of the compounds studied here, including salicylates, DCF, methotrexate and aminopterin, have long been known to elicit diverse pharmacological responses and hypersensitivities that are not completely understood in the context of the identity of their targets and mechanisms of action[27]. Our findings here suggest a possible link between such drugs or their metabolites and the function of MAIT cells and indicate a possible link between common intolerances to a drug (for example, salicylate)[31] and modulation of the activity of MAIT cells. Future work could address the clinical relevance of our observations and might call for the development of novel approaches to investigate drug-mediated effects on the activity of MAIT cells in humans.

METHODS

Methods, including statements of data availability and any associated accession codes and references, are available in the online version of the paper.

Note: Any Supplementary Information and Source Data files are available in the online version of the paper.

ACKNOWLEDGMENTS

We thank the staff at the Australian Synchrotron for assistance with data collection; the staff at the Monash Macromolecular crystallization facility; and T. Hansen (University of Washington) and W.J. Yankelevich (US Food and Drug Administration) for the 26.5 hybridoma. Supported by The University of Melbourne (S.E.), the Australian National Health and Medical Research Council (1020770 and 1027369 to D.I.G and D.P.F.; 1044215 to A.W.P.; 1113293 to J.M.; and 1125493 to J.R.), the Australian Research Council (CE140100011 and DE170100407 to S.E.; FT160100083 to A.J.C.; and FL160100049 to J.R.), the Leukaemia Foundation of Australia (N.A.G.) and Cancer Council Victoria (N.A.G.).

AUTHOR CONTRIBUTIONS

A.N.K., S.B.G.E. and W.X. designed, performed and analyzed experiments; L.L., V.A.H., J.Y.W.M., B.S.M., T.P., R.W.B., Z.C., H.W., C.D'S., L.K.-N., N.A.G., D.I.G, L.K., A.J.C. and A.W.P. performed experiments, analyzed data and/or provided key reagents for this study; and D.P.F., J.M. and J.R. supervised experiments and wrote the manuscript.

COMPETING FINANCIAL INTERESTS

The authors declare no competing financial interests.

1. Jones, E.Y., Fugger, L., Strominger, J.L. & Siebold, C. MHC class II proteins and disease: a structural perspective. *Nat. Rev. Immunol.* **6**, 271–282 (2006).
2. Koning, F., Thomas, R., Rossjohn, J. & Toes, R.E. Coeliac disease and rheumatoid arthritis: similar mechanisms, different antigens. *Nat. Rev. Rheumatol.* **11**, 450–461 (2015).
3. Illing, P.T. *et al.* Immune self-reactivity triggered by drug-modified HLA-peptide repertoire. *Nature* **486**, 554–558 (2012).
4. Godfrey, D.I., Uldrich, A.P., McCluskey, J., Rossjohn, J. & Moody, D.B. The burgeoning family of unconventional T cells. *Nat. Immunol.* **16**, 1114–1123 (2015).
5. Van Rhijn, I., Godfrey, D.I., Rossjohn, J. & Moody, D.B. Lipid and small-molecule display by CD1 and MR1. *Nat. Rev. Immunol.* **15**, 643–654 (2015).
6. Eckle, S.B. *et al.* Recognition of vitamin B precursors and byproducts by mucosal associated invariant T cells. *J. Biol. Chem.* **290**, 30204–30211 (2015).
7. Treiner, E. *et al.* Selection of evolutionarily conserved mucosal-associated invariant T cells by MR1. *Nature* **422**, 164–169 (2003).
8. Tilloy, F. *et al.* An invariant T cell receptor α chain defines a novel TAP-independent major histocompatibility complex class Ib-restricted α/β T cell subpopulation in mammals. *J. Exp. Med.* **189**, 1907–1921 (1999).
9. Salio, M., Silk, J.D., Jones, E.Y. & Cerundolo, V. Biology of CD1- and MR1-restricted T cells. *Annu. Rev. Immunol.* **32**, 323–366 (2014).
10. Gold, M.C. *et al.* Human mucosal associated invariant T cells detect bacterially infected cells. *PLoS Biol.* **8**, e1000407 (2010).
11. Le Bourhis, L. *et al.* Antimicrobial activity of mucosal-associated invariant T cells. *Nat. Immunol.* **11**, 701–708 (2010).
12. Dusseaux, M. *et al.* Human MAIT cells are xenobiotic-resistant, tissue-targeted, CD161^{hi} IL-17-secreting T cells. *Blood* **117**, 1250–1259 (2011).
13. Reantragoon, R. *et al.* Antigen-loaded MR1 tetramers define T cell receptor heterogeneity in mucosal-associated invariant T cells. *J. Exp. Med.* **210**, 2305–2320 (2013).
14. Lepore, M. *et al.* Parallel T-cell cloning and deep sequencing of human MAIT cells reveal stable oligoclonal TCRβ repertoire. *Nat. Commun.* **5**, 3866 (2014).
15. Corbett, A.J. *et al.* T-cell activation by transitory neo-antigens derived from distinct microbial pathways. *Nature* **509**, 361–365 (2014).
16. Kjer-Nielsen, L. *et al.* MR1 presents microbial vitamin B metabolites to MAIT cells. *Nature* **491**, 717–723 (2012).
17. Patel, O. *et al.* Recognition of vitamin B metabolites by mucosal-associated invariant T cells. *Nat. Commun.* **4**, 2142 (2013).
18. Ussher, J.E., Klenerman, P. & Willberg, C.B. Mucosal-associated invariant T-cells: new players in anti-bacterial immunity. *Front. Immunol.* **5**, 450 (2014).
19. Kurioka, A. *et al.* MAIT cells are licensed through granzyme exchange to kill bacterially sensitized targets. *Mucosal Immunol.* **8**, 429–440 (2015).
20. Hashkes, P.J. *et al.* Methotrexate: new uses for an old drug. *J. Pediatr.* **164**, 231–236 (2014).
21. Chatterji, D.C. & Gallelli, J.F. Thermal and photolytic decomposition of methotrexate in aqueous solutions. *J. Pharm. Sci.* **67**, 526–531 (1978).
22. Gherardin, N.A. *et al.* Diversity of T cells restricted by the MHC class I-related molecule MR1 facilitates differential antigen recognition. *Immunity* **44**, 32–45 (2016).
23. Chen, Z. *et al.* Mucosal-associated invariant T-cell activation and accumulation after in vivo infection depends on microbial riboflavin synthesis and co-stimulatory signals. *Mucosal Immunol.* http://dx.doi.org/10.1038/mi.2016.39 (4 May 2016).
24. Chua, B.Y. *et al.* The use of a TLR2 agonist-based adjuvant for enhancing effector and memory CD8 T-cell responses. *Immunol. Cell Biol.* **92**, 377–383 (2014).
25. McWilliam, H.E.G. *et al.* The intracellular pathway for the presentation of vitamin B-related antigens by the antigen-presenting molecule MR1. *Nat. Immunol.* **17**, 531–537 (2016).
26. Zelcer, S. *et al.* Methotrexate levels and outcome in osteosarcoma. *Pediatr. Blood Cancer* **44**, 638–642 (2005).
27. Romão, V.C., Lima, A., Bernardes, M., Canhão, H. & Fonseca, J.E. Three decades of low-dose methotrexate in rheumatoid arthritis: can we predict toxicity? *Immunol. Res.* **60**, 289–310 (2014).
28. Davies, N.M. & Anderson, K.E. Clinical pharmacokinetics of diclofenac. Therapeutic insights and pitfalls. *Clin. Pharmacokinet.* **33**, 184–213 (1997).
29. Krasniqi, V., Dimovski, A., Domjanović Iva, K., Bilić, I. & Božina, N. How polymorphisms of the cytochrome P450 genes affect ibuprofen and diclofenac metabolism and toxicity. *Arch. Indust. Hyg. Toxico.* **67**, 1 (2016).
30. Bharadwaj, M. *et al.* Drug hypersensitivity and human leukocyte antigens of the major histocompatibility complex. *Annu. Rev. Pharmacol. Toxicol.* **52**, 401–431 (2012).
31. Skypala, I.J., Williams, M., Reeves, L., Meyer, R. & Venter, C. Sensitivity to food additives, vaso-active amines and salicylates: a review of the evidence. *Clin. Transl. Allergy* **5**, 34 (2015).

ONLINE METHODS

***In silico* virtual screening.** Fragment-, shape- and receptor-based virtual screening was performed. In fragment-based screening, an in-house chemical database (~6,000 compounds) was searched for pyrimidines, enones, quinones, chromones (for example, flavones and isoflavones), as well as aromatic aldehydes, carboxylic acids and their derivatives, that could potentially neutralize Lys43 through Schiff base formation or ionic contacts, respectively. This search yielded 147 virtual hits, including five FDA-approved drugs (Benzbromarone, Coumarin, Menadione, Tenofovir and Thioguanine). In shape-based screening, ROCS (v 3.1.2, OpenEye Scientific Software Inc., Santa Fe, NM, http://www.eyesopen.com. OpenEye Scientific Software kindly provided the software at no cost.)[32] and Maestro Shape Screen (v 9.4, Schrödinger) were used to search for analogous shapes to 6-FP from 1,216 FDA-approved drugs (FDAMDD_v3b_1216_15Feb2008.sdf, from http://www.epa.gov/ncct/dsstox/ DataFiles.html). 2D coordinates of 1,216 drugs were converted to 3D structures with LigPrep (Schrödinger v 9.4). 16 virtual hits were obtained after visual inspection of the top 100 drugs (Combo score, ROCS; shape similarity score, Maestro), three of which were also identified in fragment-based screening (Coumarin, Menadione, and Thioguanine). In addition, Maestro Shape Screen was used to search for analogous shapes to 5-OP-RU from the same drug database (**Supplementary Fig. 1a**). In receptor-based structure screening, GOLD (v 5.1) and GLIDE (v 9.4) were used to dock a pre-filtered subset of 470 of 1,216 drugs (150 < MW < 300 Da) into the 5-OP-RU binding site of the MR1–MAIT TCR crystal structure (PDB: 4NQC). Docked ligand poses were scored with ChemPLP, Chemscore and ASPscore in GOLD and with GLIDE. Before the virtual screen, 5-OP-RU was re-docked into MR1 to reproduce its binding pose from the crystal structure and to identify scoring functions best able to predict the crystal pose (data not shown). The structure of MR1 K43A (PDB accession code, 4NQD) was chosen for re-docking 5-OP-RU, as there was no covalent bond to MR1. For the virtual screen, the active site was defined by a 10 Å radius around Arg9 and a rigid MR1 conformation was used for ligand docking. The top scoring 200 drugs were analyzed by visual inspection for ligand-protein interactions simulated from docking. To increase the hit rate, another docking program, GLIDE, was also used in Standard Precision docking mode to score ligand binding using GScore. The active site was the same for GLIDE and GOLD docking. In total 20 drug hits were selected for screening, one of which was also identified via fragment-based screening (Thioguanine).

Aminopterin photodegradation. Aminopterin powder (Sigma-Aldrich) was dissolved in phosphate-buffered saline (pH 8.5) at a concentration of 0.5 mg/ml and exposed to light produced by a 2 × 38W fluorescent lamps at a distance of 40 cm at room temperature. The degree of photodegradation was monitored using the method previously described[33], whereby the absorbance spectrum was analyzed over 230–480 nm using a PHERAstar plate reader (BMG labtech). The photodegradation reaction was deemed nearly complete after 48 h, which was subsequently confirmed by HPLC analysis against undegraded sample (data not shown). The effect of degraded aminopterin on MR1 surface expression of C1R.MR1 cells was performed as described previously[34] using biotinylated monoclonal antibody (mAb) 26.5 (purified from hybridomas in ref. 41 and biotinylated in-house; dilutions optimized individually) and streptavidin-PE (BD Biosciences). Cells were treated for 3 h before staining, flow cytometry analysis was carried out using a CyAn ADP (Beckman Coulter) and produced data were analyzed using FlowJo v10.1.

Compounds tested in cellular assays *in vitro* and *ex vivo*. 6-FP and Ac-6-FP (Schircks Laboratories) were dissolved at 5 mM in water, supplemented with 17 mM NaOH. 5-OP-RU (as 1.52 mM stock solution in DMSO) was used by dilution in PBS to the required concentration immediately before testing (DMSO content was less than 0.01% in final media). All other compounds were obtained commercially (Sigma-Aldrich, Fluka or Sapphire Bioscience) or were synthesized in house and dissolved at 50 mM in DMSO. All compounds were diluted in PBS. For inhibitory compounds, vehicle controls (V) were prepared as follows: V1 of ligands prepared at 5 mM in water supplemented with 17 mM NaOH; V2 of ligands prepared at 50 mM in DMSO.

Cell lines, peripheral blood mononuclear cells (PBMCs) and monocyte-derived dendritic cells. All cells were cultured in RPMI medium supplemented with 10% FCS and serum complement (RF10 medium). Clonal C1R cells overexpressing MR1 (CIR.MR1)[35] or HLA-B*08:01 (ref. 36) have been described previously and were derived from C1R (ATCC number CRL-1993), a human B lymphoblastoid cell line (LCL). Clonal Jurkat.MAIT cells expressing the TRBV6-1 A-F7 MAIT TCR (Jurkat.MAIT-A-F7), the TRBV6-4 #6 MAIT TCR (Jurkat.MAIT-#6) or the TRBV20 C-F7 MAIT TCR (Jurkat.MAIT-CF7)[15] or the LC13 TCR and CD8αβ (Jurkat.CD8.LC13)[36] have been described previously and were derived from the human T cell line Jurkat RT3-T3.5 (Jurkat; ATCC number T1B-153). Clonal Jurkat76.MAIT-A-F7 (ref. 15), bulk sorted Jurkat76.CD3.MAV21, Jurkat76.CD3.MAV36, Jurkat76.CD3.MBV28 (ref. 22) have been described previously and were derived from the human T cell line Jurkat76 (ref. 37). Bulk-sorted SKW-3.M12-64 and SKW-3.M20-64 cells[22] have been described previously and were derived from the human T cell line SKW-3 (DSMZ accession code ACC-53). For the generation of Bw58.CD3.MAIT-V_β8.2 cells, sequential retroviral transduction with genes encoding CD3 and TCR was performed as described previously[38]. In brief, genes encoding full-length CD3 (CD3 γ-, δ-, ζ- and ε-chains) were designed, purchased and cloned into a self-cleaving 2A-peptide-based (MSCV)-IRES-GFP (pMIG) vector[39]. After sequence verification, mouse-CD3-encoding genes were transduced into the TCR-deficient Bw58 cells. GFP^{hi} cells (Bw58.CD3) were cloned by single-cell flow cytometry. Similarly, genes encoding full-length MAIT TCRs of a V_β8.2 TCR derived from a mouse with transgenic expression of a TCR using the canonical V_α19i segment (V_α19i $C\alpha^{-/-}$)[40] and the endogenous paring TCR β-chain (TRBV13-2*01 (Arden nomenclature V_β8.2), TRBJ2-3*01, CDR3β CASGDAKLGVGAETLYF)) were cloned into pMIG vector and the sequence was verified, and then these were transduced into Bw58.CD3 cells to generate Bw58.CD3.MAIT-Vβ8.2 cells. Similarly bulk sorted Jurkat.76.CD3.AM1, Jurkat.76.CD3.AM2, Jurkat.76.CD3.AM3 and bulk-sorted SKW-3.M33-20 cells were generated based on TCR sequences described previously[22]. For the generation of high-level MR1-expressing antigen-presenting cells (M12.C3.MR1), the same retroviral system was used. M12.C3 cells (an MHC-class-II-deficient B-lymphoblastoid cell line) were transduced with mouse MR1 (pMIG-MR1) and clones were generated by single-cell flow cytometry. PBMCs were isolated from whole blood of healthy donors and stored in liquid nitrogen (authorized by the Australian Red Blood Cross Service Material Supply Agreement with The University of Melbourne) as described previously[13]. Monocyte-derived dendritic cells (mDCs) were generated from PBMCs by incubating plastic-adherent PBMCs for 5 d in RF10 media supplemented with 300 U/ml hGM-CSF (Peprotech) and 100 U/ml hIL-4 (Peprotech). Plastic-non-adherent PBMCs were refrozen in liquid nitrogen and thawed out 1 d before addition to mDCs as autologous lymphocytes in activation assays.

Activation of human and mouse T cell lines. Human MR1-reactive T cell lines (1×10^5 cells) were tested for activation by co-incubation with vehicle controls, PBS and medium alone (background) or doses of compounds in the presence of C1R.MR1 cells (1×10^5) for 16 h in 200 µl RF10 medium. To test if inhibitors affected the ability of the T cell lines to be activated, cells were incubated with PMA (phorbol 12-myristate 13-acetate) and ionomycin (final concentration of 10 ng/ml and 1 µg/ml, respectively) and the highest concentration of inhibitor. In addition, a T cell line (Jurkat.CD8.LC13) restricted by a MHC class I molecule (HLA-B*08:01) was co-incubated with its cognate peptide FLRGRAYGL (FLR, 1 µM) and each of the compounds. Cells were subsequently stained with the mAbs anti-CD3-PE-Cy7 (clone UCHT1, eBioscience, 1:50), and anti-CD69-APC or anti-CD69-PE (clone FN50, BD Biosciences, 1:50), as well as anti-CD19-APC-Cy7 (clone SJ25C1, BD Biosciences, 1:100), in the case of bulk sorted T cell lines (to distinguish antigen presenting cells), and 7AAD (BD Biosciences) for 30 min on ice, washed twice with flow cytometry wash (2% FCS in PBS) and fixed with flow cytometry fix (2.1% glucose and 1% paraformaldehyde in PBS), and data were acquired on a BD FACSCanto II or LSR Fortessa flow cytometer and analyzed using FlowJo. Activation of T cell lines was measured by an increase in surface CD69 expression of $CD3^+GFP^{lo}$ cells (clonal T cell lines) or $CD3^+CD19^-$ cells (bulk sorted T cell lines) and MFI CD69 relative to background was calculated.

Jurkat76.MAIT-A-F7 or Bw58.CD3.MAIT-Vβ8.2 cells (1×10^5) were tested for activation by co-incubation with vehicle controls, PBS (background), doses of compounds and C1R.MR1 cells or M12.C3.MR1 cells (1×10^5) for 24 h in 200 µl RF10 medium. To test if inhibitors do not affect the ability of the

doi:10.1038/ni.3679

T cell lines to produce IL-2, cells were incubated with PMA and ionomycin (final concentration of 10 ng/ml and 1 μg/ml respectively) and the highest concentration of inhibitor. IL-2 production was measured as a mean of T cell activation in ELISA (human: BD Biosciences OptEIA kit, mouse: mAb IL-2 (clone JES6-1A12, BD Biosciences, 1:500) using 100 μl of supernatant, frozen and thawed to kill cells. In brief, IL-2 was assayed with biotinylated mAb to IL-2 and *o*-Phenylenediamine dihydrochloride (OPD; Sigma-Aldrich) substrate conversion by HRP-Streptavidin detected at 492-nm emission and IL-2 concentrations calculated based on IL-2 standards. For inhibition, inhibiting compounds were added to antigen-presenting cells for 15 min before the addition of 5-OP-RU and T cells. For MR1 blocking, mAb 26.5 (ref. 41) (antibody purified in house from hybridoma provided by T. Hansen (University of Washington) and W.J. Yankelevich (US Food and Drug Administration)) or isotype-matched control mAb (8A5, made in house and specific for the human pre-TCR α-chain) were added at 20 μg/ml for 1 h to antigen-presenting cells before addition of T cells.

To determine the half-maximum inhibition by inhibitory compounds (IC_{50} values), background activation levels were subtracted, data normalized, inhibitor concentrations transformed to log and nonlinear regression of log (inhibitor) versus the normalized response determined using Prism software.

All cell lines tested negative for mycoplasma. While SKW-3 cells are listed on the database of cross-contaminated or misidentified cell lines, where they are described as being contaminated with the KE-37 line, we have transfected specific TCR-encoding genes into these cells, which we then recloned and/or enriched by iterative cell sorting for TCR expression. Following these steps the cells were then validated for antigen recognition of cognate antigens in activation experiments.

Detection of upregulation of MR1 on the cell surface. C1R.MR1 cells (1×10^5) were incubated for various times (**Fig. 2c**) with vehicle controls, PBS and medium (background), and 100 μM of compounds in 200 μl RF10 medium per well. Then cells were stained with biotinylated mAb 26.5 (anti-MR1)[41] (identified above, dilution 1:1,000) or biotinylated isotype-matched control mAb (8A5; identified above) on ice for 30 min, washed twice with flow cytometry wash, and then stained with Streptavidin-PE (BD Biosciences) and 7AAD (BD Biosciences) on ice for 30 min, washed twice again and fixed by flow cytometry, and data were acquired on a BD LSR Fortessa flow cytometer and analyzed using FlowJo. MR1 upregulation was measured by an increase in 26.5 staining of GFP^{hi} cells (C1R.MR1), and the MFI of 26.5 relative to background was calculated.

Cellular screening of compounds for MR1 upregulation and Jurkat.MAIT cell activation. Sets of drugs and other small molecules were tested in a combined assay of the activation of MAIT cells and upregulation of MR1 expression, whereby C1R.MR1 cells (1×10^5) and Jurkat.MAIT-A-F7 cells (1×10^5) were co-incubated with 100 μM and 10 μM of each compound as described above. Each time, the activation of Jurkat.MAIT-A-F7 cells by 10 nM 5-OP-RU and upregulation of MR1 expression by 100 μM 6-FP were included as positive controls and PBS was included as a background control. Cells were stained first with biotinylated mAb 26.5 (anti-MR1; identified above (ref. 41), dilution 1:1,000), anti-CD3-PE-Cy7 (clone UCHT1, eBioscience, dilution 1:50), and anti-CD69-APC (clone FN50, BD Biosciences, dilution 1:50) on ice for 30 min, washed three times with flow cytometry wash, and then stained with Streptavidin-PE (BD Biosciences), 7AAD (BD Biosciences) on ice for 30 min, washed twice again and fixed by flow cytometry, and data were acquired on a BD FACSCanto II flow cytometer and analyzed using FlowJo. To allow for comparison between experiments, results relative to background was normalized by setting the % CD69 upregulation by 10 nM 5-OP-RU or % MR1 upregulation by 100 μM 6-FP equal to 100% and results relative to a background of 1 equal to 0%. Compounds that caused activation of Jurkat.MAIT cells and upregulation of MR1 expression greater than 75% at 100 μM and/or 25% at 10 μM compound were considered agonistic and strongly MR1 upregulating, respectively, and those that caused such activation and upregulation greater than 7.5% and less than 75% at 100 μM and/or larger than 7.5% and less than 25% at 10 μM compound were considered weakly agonistic and weakly MR1 upregulating, respectively. For some of the small molecules tested at 100 μM, we observed a toxic effect that resulted in cell death identified by life-dead stain. In these cases, MR1 upregulation was more pronounced at a lower concentration of inhibitor (10 μM) than at 100 μM, for example, 5-hydroxy-1,4-naphtoquinone. Considering MR1 upregulation at 10 μM as part of the selection criteria in such cases thus allowed inclusion of molecules that appeared toxic at 100 μM.

***Ex vivo* activation of human PBMCs assayed by intracellular cytokine staining.** Per sample to mDCs (1×10^5), PBS (background), vehicle controls and doses of inhibitors were added, followed after 15 min by PBS or titrating amounts of 5-OP-RU. Then autologous lymphocytes (0.5×10^6) were added per sample. To test if inhibitors affected the ability of cells to produce cytokines, autologous non-plastic-adherent PBMCs were incubated with PMA and ionomycin (final concentrations of 100 ng/ml and 10 μg/ml, respectively) and the highest concentration of inhibitor. Upon incubation for 1 h, brefeldinA (final concentration of 10 μg/ml) was added and incubation continued for 6 h, then surface stained for 20 min at room temperature (Zombie Yellow Fixable Viability Kit, Biolegend, dilution 1:500); anti-CD3-PE-CF594 (clone UCHT1, BD Biosciences, dilution 1:200); anti-TRAV1-2-APC (clone 3C10, Biolegend, dilution 1:50); human MR1–5-OP-RU tetramer, generated as described previously[15], followed by adding PFA (final concentration of 1%) and a 20 min incubation at RT, washed twice with PBS and stained intracellularly (anti-IFN-γ-FITC (clone 25723.11, BD Biosciences, dilution 1:40); anti-TNFα-Pacific Blue (clone Mab11, Biolegend), dilution 1:200) in 0.3% Saponin in PBS overnight at 4 °C. The next day, cells were washed twice in PBS and data was acquired using a BD LSR Fortessa flow cytometer and analyzed by FlowJo. Percent inhibition was calculated as 100 − (a/b × 100), where 'a' represents activation by 5-OP-RU in the presence of an inhibitor, whereby the background 'b' (% cytokine production/% CTV dilution in the presence of inhibitor only (without 5-OP-RU), is subtracted.

***Ex vivo* activation of human PBMCs assayed by proliferation.** Autologous lymphocytes and mDCs were stained with CellTrace Violet (Molecular Probes) according to the manufacturer's protocol. Per sample to mDCs (1×10^5), PBS (background), vehicle controls and doses of inhibitors were added, followed after 15 min by PBS or titrating amounts of 5-OP-RU. Then autologous lymphocytes (1×10^6 per sample) were added. To test if inhibitors affected the ability of cells to produce cytokines, autologous non-plastic-adherent PBMCs were incubated for 48 h with plate-bound mAb to CD3 (clone OKT3, 10 μg/ml, prepared in-house) plus anti-CD28 (clone L293, BD Biosciences, 2 μg/ml) and the highest concentration of inhibitor in a flat-bottom plate before transfer to a U-shape plate after 48 h. Upon incubation of 5 d, samples were stained for 20 min at room temperature (Zombie Yellow Fixable Viability Kit (Biolegend), dilution 1:500), followed by staining for surface markers as above in the case of intracellular cytokine staining. Samples were washed twice with flow cytometry wash and fixed and data were acquired using a BD LSR Fortessa flow cytometer and analyzed by FlowJo. Percent inhibition was calculated as described above for intracellular cytokine staining.

Mouse *in vivo* activation or inhibition of the accumulation of MAIT cells in the lungs. *Salmonella* enterica serovar Typhimurium BRD509 (Salm.BRD509) has been previously described[42]. Salm.BRD509 harbors deletions in *aroA* and *aroD* that resulting in limitation of replication and spread of bacteria and has an intact riboflavin synthesis pathway. The BRD509Δ*ribDH* mutant (Salm. BRD509Δ*ribDH*), lacking a gene segment containing *ribD* and *ribH*, which encode key enzymes in the riboflavin-synthesis pathway, was constructed by lamda red-recombinase mediated allelic replacement followed by transduction using phage P22 as previously described[15]. BRD509Δ*rib*DH cultures were supplemented with 20 μg/ml riboflavin. Bacteria were cultured at 37 °C statically, in Luria Bertani broth (LB) for 16–18 h to log-phase growth (OD_{600} 0.6–0.9) in the presence of antibiotics (30 μg/ml streptomycin, 30 μg /ml kanamycin) and riboflavin (20 μg/ml). For the infecting inoculum, bacteria were re-inoculated in pre-warmed medium for a further 2-4 h static culture (OD_{600} 0.4–0.6). With the estimation that 1 $OD_{600} = 5 \times 10^8$/ml, sufficient bacteria were washed and diluted in PBS for intranasal delivery to C57BL/6 mice. A sample of inoculum was plated onto Luria agar supplemented with antibiotics and riboflavin for verification of bacterial concentration by counting colony-forming units.

Mice were bred and housed in the Biological Research Facility of the Peter Doherty Institute. Male mice 7–8 weeks of age were used in experiments and allocated to separate groups at random (block randomization). The investigators were blinded to the group allocation when assessing the outcome. All procedures were approved by The University of Melbourne Animal Ethics Committee. Mice were intranasally inoculated using a total volume of 50 µl with Ac-6-FP (5×10^4 pmol and titrations in PBS plus 1% DMSO) or 3-F-SA (5×10^5 pmol and titrations in PBS plus 1% DMSO) at day −2 and day −1 or, alternatively, with vehicle control (PBS plus 1% DMSO). On day 0, mice were inoculated intranasally with BRD509Δ*ribDH* (2×10^7 cfu) and 5-OP-RU (3 pmol in PBS of a 14.1 mM stock in DMSO) and/or inhibitory antigens (or vehicle control) in 50 µl per nares. Then, on day 1, day 2 and day 4, mice were inoculated intranasally with 5-OP-RU and/or inhibitor using a total volume of 50 µl. All inoculations were performed on mice anesthetized by isoflurane with an anaesthetizing machine. At day 7, mice were killed by administration of CO_2 and lungs (following heart perfusion with 10 ml cold RPMI) were harvested. To prepare single-cell suspensions, lungs were finely chopped with a scalpel blade and treated with 3 mg/ml collagenase III (Worthington), 1 mg/ml DNase and 2% FCS in RPMI for 90 min at 37 °C with gentle shaking. Cells were then filtered (70 µM) and washed with flow cytometry wash. Red blood cells were lysed from lung preparations with hypotonic buffer TAC (Tris-based Amino Chloride) for 5 min at RT and approximately 1.5×10^6 cells were filtered (40 µm) and prepared for staining. To block non-specific staining, cells were incubated with mouse MR1–6-FP tetramer (1:100) diluted in 20 µl of supernatant of hybridoma 2.4G2 (ATCC HB-197) as anti-Fc receptor (2.4G2 hybridoma, grown to a density of 1×10^6 to 1.5×10^6 cells per ml culture; prepared in-house) for 15 min at RT. Cells were then incubated at RT for 30 min with antibodies (from BD) specific for CD19 (clone 1D3, dilution 1:200), CD45.2 (clone 104, dilution 1:200) and TCRβ (clone H57-597, dilution 1:200), as well as 7AAD (1:500) and mouse MR1–5-OP-RU tetramer[13], in flow cytometry wash. Cells were fixed with 1% PFA in PBS and 25- to 30-k blank calibration particles (BD) were added to enumerate absolute cell numbers, before analysis on a BD LSR Fortessa flow cytometer.

For intracellular cytokine staining, Golgi Plug (BD Biosciences) was used during all processing steps. Cells stimulated with PMA and ionomycin (20 ng/ml and 1 µg/ml, respectively) for 4h at 37 °C were included as positive controls alongside non-stimulated samples. Surface staining was performed as above, followed by intracellular cytokine staining for IL-17A (clone TC11-18H10, BD Biosciences, dilution 1:200) using the BD Fixation/Permeabilization Kit according to the manufacturer's instructions. Data analysis was performed with FlowJo software.

Generation of soluble proteins for crystallography. Soluble A-F7 MAIT TCR and MR1–β_2-microglobulin (β_2m) were folded from inclusion bodies and purified using methods based on those described previously[17]. MR1, β_2m, TCR α-chain and TCR β-chain were overproduced separately as insoluble inclusion bodies in *Escherichia coli* BL21(DE3) that had been transformed with pET plasmid containing gene of interest. Protein overproduction was induced in *E. coli* cells, cultured in LB media that had reached an optical density of 0.5, by the addition a 0.5 µM IPTG, and further culturing for 4 h at 37 °C with shaking. Cells were harvested by centrifugation and lysed by resuspending in 1% (v/v) Triton-X, 4 mM $MgCl_2$, 10 mM DTT, 1 g/l lysozyme (Sigma-Aldrich) and 0.5 g/l DNase, and incubating for 2 h at room temperature. Inclusion bodies were harvested from the lysate by centrifugation, before being washed 4 times in 50 mM Tris (pH 8), 0.5% (v/v) Triton-X, 100 mM NaCl and 1 mM EDTA, omitting the Triton-X and NaCl from the final wash step. Lastly, the isolated inclusion bodies were resuspended in 20 mM Tris (pH 8), 6 M guanidinium, 0.5 mM EDTA and 1 mM DTT. The approximate concentration and purity of the isolated inclusion bodies was estimated using SDS-PAGE.

The MAIT TCR was refolded by rapidly diluting 63 mg of α-chain and 42 mg of β-chain as inclusion bodies, into 500 ml of 100 mM Tris (pH 8.5), 2 mM EDTA, 0.4 M L-arginine, 5 M urea 0.5 mM oxidized glutathione, 5 mM reduced glutathione and 1 mM PMSF. Additionally, MR1-β_2m bound to the compounds, HMB or 3-F-SA was refolded by rapidly diluting 56 mg of MR1 and 26 mg of β_2m as inclusion bodies, into 400 ml of this same refold buffer described above but with the addition of 5 mg/l of the target compound. For 2,4-DA-6-FP, the refold contained 10 mg/ml of aminopterin that had been photodegraded for 18 h. All refold samples were stirred for 14 h at 4 °C, before dialyzing three times against 15 l of 10 mM Tris (pH 8). Dialysate was passed through Macro-Prep DEAE resin (Bio-Rad) and protein was eluted using 10 mM Tris (pH 8) with 400 mM NaCl. Next, the eluate was concentrated down to 3 ml and purified by size exclusion chromatography using AKTA purification system and a Superdex200 15/60 column (GE Healthcare). Finally, the purified sample was passed over a HiTrap-Q HP (GE Healthcare) and eluted in 10mM Tris (pH8) using a gradient of 0 mM to 300 mM NaCl over 20 CV. Purified protein was assessed for purity using SDS-PAGE and concentrations were calculated from A_{280} values measured using a NanoDrop-spectrophotometer (Thermo-fisher).

Crystallization and structure determination. Purified MR1-β_2m-antigen was mixed with purified MAIT TCR in a 1:1 molar ratio and concentrated to a final concentration of 5 mg/ml. Samples were crystallized by hanging-drop vapor diffusion by mixing protein 1:1 with precipitant consisting of 100 mM BTP (pH 6–6.5), 8–20% (w/v) PEG3350 and 200 mM sodium acetate, as established previously[17]. Crystals formed over 1–5 d at 21 °C. Diffraction data was collected at 100K on the Australian synchrotron MX1 and MX2 beamlines, from crystals that had first been washed in precipitant solution augmented with 10% (v/v) glycerol for cryo-protection. Measured reflections were indexed and integrated using either XDS[43] or imosflm, and scaled and merged using aimless[44]. Phases were calculated by molecular replacement using PHASER[45], whereby, the MR1 ternary complex, which had the CDR loops and ligand removed, was used as a search model (PDB accession code, 4L4T)[17]. Refinement was performed using phenix.refine[46], with the initial refinement rounds including simulated annealing, model building was performed with COOT[47], with MolProbity used in validation[48]. The Grade Web Server was used to generate ligand restraints for all drugs.

For the compounds DCF, 5-OH-DCF and 2-OH-1-NA, which did not refold sufficiently well *in vitro* (data not shown), a ligand-exchange approach was employed to obtain structures of MR1 presenting these molecules: when 6-FP (data not shown), DCF, 5-OH-DCF or 2-OH-1-NA was added to the MAIT TCR–MR1–antigen protein solution at a concentration of 0.6-2 mM before crystallization, the resulting crystal structures determined from these crystals revealed the added compound at a high occupancy (**Fig. 5**). The buried surface area was calculated by the CCP4 implementation of Areaimol and molecular interactions were determined by the CCP4 implementation of CONTACT[44]. All molecular graphics were constructed using PyMOL.

Mass spectrometry. C1R.MR1 cells (5×10^9) were treated with Ac-6-FP, 3-F-SA or DCF for 3 h and 16 h, after which the cells were washed extensively and the cell pellet was 'snap frozen' in liquid nitrogen. The plasma membrane from treated cells was then isolated using an AbCAM plasma membrane kit (product number ab65400). MR1 was isolated from the plasma membrane fraction by immunoprecipitation using 50 µg of mAb 26.5 (identified above) that was pre-coupled to 100 µl protein G-agarose. MR1 and bound ligands were eluted from the resin by acidification and ligand containing fractions were further purified by solid phase extraction using a C_{18} (Waters) or SAX (Supel Co.) stationary phase for DCF and 3-F-SA respectively. Components of interest were eluted from cartridges with 1 ml of methanol. Eluted components were dried on a SpeedVac dryer (Thermo Electron, Waltham, MA). The dried samples were resuspended in 50 µl of water/acetonitrile (95:5) for MS/MS analyses.

LC-MSMS for profiling of synthetic standards. Standards were subjected to chromatographic separations with a micropeptide trap (Grace Scientific) connected to an Everest C18 column (50 mm × 1 mm, 5 µm, Grace Davison) and a Bruker microQTOF mass spectrometer. The starting mobile phase consisted of 95% water (0.5% acetic acid, 10 mM ammonium acetate), and the metabolites were eluted using a linear gradient of 95% water to 85% acetonitrile over 25 min at a flow rate of 50 µl/min. Mass spectra were collected in positive ionization mode by scanning over the range m/z 50 to 500.

Targeted detection of compounds using multiple reaction monitoring (MRM)-MS. A SCIEX QTRAP 5500 mass spectrometer was used for MRM detection of compounds. 20-µl samples were injected and loaded onto a trap

doi:10.1038/ni.3679

column (200 µm × 0.5 mm ChromXP C18-CL 3 µm 120 Å) at a flow rate of 10 µl/min in 98% buffer A for 10 min. For on-line fractionation of samples onto the mass spectrometer, samples were eluted from the trap column and over a cHiPLC column (75 µm × 15 cm ChromXP C18-CL 3 µm 120 Å) at 300 nl/min under the following gradient conditions for buffer B (95% acetonitrile, 0.1% formic acid in water): 0–3 min in 2–10% B, 3–33 min in 10–40% B, 33–36 min in 40–80% B, 36–38 min hold at 80% B, 38–39 min in 80–2% B, followed by equilibration at 2% B until the end of the run at 48 min. The QTRAP 5500 was operated in MRM mode in unit resolution for Q1 and Q3, coupled to an information-dependent acquisition (IDA) criterion set to trigger an enhanced product ion scan (10,000 Da/sec; rolling CE; unit resolution) following any MRM transition exceeding 500 counts (ignoring the triggering MRM transition for 3 s thereafter).

For comparison of DCF from cell surface, transitions were simultaneously monitored in detecting DCF Q1 to Q3: *m/z* 295→250, 4-OH-DCF *m/z* 312.0→266, 312→230, and 312→194 and 5-OH-DCF *m/z* 312→266, 312→230, 4′,5-dihydroxy-DCF 327.9→290, 327.9→282, 327.9→246, 325.7→210. Two transitions were simultaneously monitored in detecting Ac-6-FP Q1 to Q3: *m/z* 234.1→190.1, *m/z* 234.1→147.1 and 3-F-SA detecting Q1 to Q3: *m/z* 165.1→120.9 *m/z* 165.1→92.9. Data analysis was performed using Analyst v1.5.2.

Chemical synthesis. 2,4-DA-6-FP, 4′,5-diOH-DCF, and 5-OH-DCF were synthesized as shown in **Supplementary Figure 8**.

Statistical analysis. Where appropriate, data are presented as mean ± standard error.

Data availability. The data that support the findings of this study are available from the corresponding author upon request. Structural information has been deposited in PDB under accession codes: 5U16, 5U17, 5U1R, 4U6Q, 5U2V and 5U72.

32. Hawkins, P.C.D., Skillman, A.G. & Nicholls, A. Comparison of shape-matching and docking as virtual screening tools. *J. Med. Chem.* **50**, 74–82 (2007).
33. Fehlner, P.F., Bencsath, A., Lam, T. & King, T.P. The photodecomposition of aminopterin. *J. Immunol. Methods* **101**, 141–145 (1987).
34. Eckle, S.B. *et al.* A molecular basis underpinning the T cell receptor heterogeneity of mucosal-associated invariant T cells. *J. Exp. Med.* **211**, 1585–1600 (2014).
35. Reantragoon, R. *et al.* Structural insight into MR1-mediated recognition of the mucosal associated invariant T cell receptor. *J. Exp. Med.* **209**, 761–774 (2012).
36. Gras, S. *et al.* The shaping of T cell receptor recognition by self-tolerance. *Immunity* **30**, 193–203 (2009).
37. Heemskerk, M.H.M. *et al.* Redirection of antileukemic reactivity of peripheral T lymphocytes using gene transfer of minor histocompatibility antigen HA-2-specific T-cell receptor complexes expressing a conserved α joining region. *Blood* **102**, 3530–3540 (2003).
38. Gras, S. *et al.* Allelic polymorphism in the T cell receptor and its impact on immune responses. *J. Exp. Med.* **207**, 1555–1567 (2010).
39. Szymczak, A.L. *et al.* Correction of multi-gene deficiency *in vivo* using a single 'self-cleaving' 2A peptide-based retroviral vector. *Nat. Biotechnol.* **22**, 589–594 (2004).
40. Kawachi, I., Maldonado, J., Strader, C. & Gilfillan, S. MR1-restricted V alpha 19i mucosal-associated invariant T cells are innate T cells in the gut lamina propria that provide a rapid and diverse cytokine response. *J. Immunol.* **176**, 1618–1627 (2006).
41. Huang, S. *et al.* Evidence for MR1 antigen presentation to mucosal-associated invariant T cells. *J. Biol. Chem.* **280**, 21183–21193 (2005).
42. Hoiseth, S.K. & Stocker, B.A.D. Aromatic-dependent Salmonella typhimurium are non-virulent and effective as live vaccines. *Nature* **291**, 238–239 (1981).
43. Kabsch, W. XDS. *Acta Crystallogr. D Biol. Crystallogr.* **66**, 125–132 (2010).
44. Winn, M.D. *et al.* Overview of the CCP4 suite and current developments. *Acta Crystallogr. D Biol. Crystallogr.* **67**, 235–242 (2011).
45. McCoy, A.J. *et al.* Phaser crystallographic software. *J. Appl. Crystallogr.* **40**, 658–674 (2007).
46. Adams, P.D. *et al.* PHENIX: a comprehensive Python-based system for macromolecular structure solution. *Acta Crystallogr. D Biol. Crystallogr.* **66**, 213–221 (2010).
47. Emsley, P., Lohkamp, B., Scott, W.G. & Cowtan, K. Features and development of Coot. *Acta Crystallogr. D Biol. Crystallogr.* **66**, 486–501 (2010).
48. Chen, V.B. *et al.* MolProbity: all-atom structure validation for macromolecular crystallography. *Acta Crystallogr. D Biol. Crystallogr.* **66**, 12–21 (2010).